Field Trials for Cost-Effective Strengthening of SC Load Posted Bridges

FINAL REPORT

Prepared by:

Dr. Paul Ziehl

Professor, Departments of Mechanical and Civil and Environmental Engineering

University of South Carolina

Dr. Tommy Cousins

Professor, Glenn Department of Civil Engineering

Clemson University

Dr. Brandon Ross

Professor, Glenn Department of Civil Engineering

Clemson University

Dr. Fabio Matta

Professor, Department of Civil and Environmental Engineering

University of South Carolina

FHWA-SC-26-03

August 2026

Sponsoring Agencies:

South Carolina Department of Transportation

Office of Materials and Research

1406 Shop Road

Columbia, SC 29201

Federal Highway Administration

South Carolina Division

Strom Thurmond Federal Building

1835 Assembly Street, Suite 1270

Columbia, SC 29201

Technical Report Documentation Page

1. Report No FHWA-SC-26-03	2. Government Accession No.	3. Recipient's Catalog No.
4. Title and Subtitle *Field Trials for Cost-Effective Strengthening of SC Load Posted Bridges*		5. Report Date *August 2026* 6. Performing Organization Code
7. Author/s *Drs. Paul Ziehl, Tommy Cousins, Brandon Ross, Fabio Matta*		8. Performing Organization Report No.
9. Performing Organization Name and Address *University of South Carolina* *Dept. of Civil and Environmental Engineering* *300 Main Street, Columbia, SC 29208*		10. Work Unit No. (TRAIS) 11. Contract or Grant No. SPR No. 758
12. Sponsoring Organization Name and Address South Carolina Department of Transportation Office of Materials and Research 1406 Shop Road Columbia, SC 29201		13. Type of Report and Period Covered *Interim Report* 14. Sponsoring Agency Code
15. Supplementary Notes		

16. Abstract

The transportation infrastructure in South Carolina includes many bridges that are load posted due to structural considerations (e.g., outdated design loads, members whose capacity is difficult to assess) resulting in substantial costs to the public. The significant number of posted bridges has an adverse effect on travel and commerce in South Carolina. Efficient bridge strengthening methods are described in this report to mitigate these effects. This report focuses on laboratory and field trials of strengthening methods for precast flat slab and channel girder bridges. The goal is provide a means for reducing the number of load-posted bridges through efficient strengthening.

Strengthening methods were investigated and laboratory testing was conducted to verify the structural response pre- and post-strengthening. A cost evaluation of the most suitable strengthening methods was performed and selected solutions verified through field implementation and load testing.

The outcomes of this research are expected to provide efficient means to minimize the number of load-posted bridges. The work described is part of a larger effort to extend the service life of bridges in South Carolina.

17. Key Words *Bridge evaluation; precast flat slabs; channel girders;; strengthening; load rating*	18. Distribution Statement No restrictions. This document is available to the public through the National Technical Information Service, Springfield, VA 22161.		
19. Security Classification (of this report) Unclassified	20. Security Classification (of this page) Unclassified	21. No. Of Pages 92	22. Price None.

Form DOT F 1700.7 (8-72) Reproduction of form and completed page is authorized.

DISCLAIMER

The contents of this report reflect the views of the authors who are responsible for the facts and the accuracy of the data presented herein. The contents do not necessarily reflect the official views or policies of the South Carolina Department of Transportation or the Federal Highway Administration. This report does not constitute a standard, specification, or regulation.

The State of South Carolina and the United States Government do not endorse products or manufacturers. Trade or manufacturer's names appear herein solely because they are considered essential to the object of this report.

ACKNOWLEDGMENTS

The authors wish to acknowledge the useful and insightful input from the Project Steering Committee, including Terry Swygert, Sean Futch, William Munnerlyn, Merrill Zwanka, Daniel Cook, Blake Gerken, Josh Quattlebaum, and Michael Turner. Special thanks are extended to Rodrick Tucker, the Chair of the PSC and Mark Hunter, who was critical to the development of the project approach.

Li Ai and Mehdi Shahzamanian, Research Assistant Professors at the University of South Carolina, assisted with research efforts and report writing.

Laboratory Technicians at USC and Clemson supported lab and field work. The efforts of Scott Black, Caleb Jackson, and Russell Inglett are gratefully acknowledged.

Many graduate and undergraduate students assisted with the field and lab studies. University of South Carolina students include Ryan Budke and Laxman KC. Clemson students include Jacob Bowers, Sam Dodd, Coleman Eubanks, Aashish Sapkota, and Paige Waters.

In-kind donations of time and materials were provided by Metromont LLC, Modified Concrete Suppliers LLC, and V2 Composites Inc.

Assistance from SCDOT maintenance personnel from Districts 2 and 6 was essential to the project. William Munnerlyn and crews from District 2 assisted with the acquisition and delivery of skinny-leg channel test specimens and supported the retrofit and field testing conducted on the Airport Road Bridge in Greenwood, SC. Field testing and retrofitting of the Four Hole Swamp Bridge in Dorchester County were supported by Michael Turner and the District 6 crews.

EXECUTIVE SUMMARY

The transportation infrastructure in South Carolina includes many bridges that are load-posted due to structural considerations (e.g., outdated design loads, members whose capacity is difficult to assess), resulting in substantial costs to the public. Previous research projects, including SPR 752 – Safe and Cost-Effective Removal of Load Postings for South Carolina Bridges, have helped to cost effectively reduce the number of load postings in South Carolina without the need for strengthening. In some cases, bridge superstructure systems will still require strengthening to achieve a sufficient load rating value. This report documents the exploration, selection and implementation of cost-effective and rapidly deployable bridge strengthening methods.

The South Carolina Department of Transportation recently completed a multi-year effort to load rate its inventory of over 9,400 bridges. Findings from the effort identified both precast flat slabs and prestressed concrete channel girders (referred to as "channel girders" hereafter) as superstructure types of interest. Many precast flat slabs and channel girder bridges are understrength with respect to rating vehicles and will require intervention in the form of posting, strengthening, or replacement. This report addresses laboratory testing and field trials of strengthening methods for these bridge types.

Channel girders in SC bridges are informally described as 'skinny leg' or 'wide leg' depending on their web thickness. Skinny leg channel girders are generally in worse condition than wide leg channel girders and were the focus of this project. The baseline structural response of skinny leg channel girders salvaged from decommissioned bridges was assessed in the laboratory through full-scale load tests. Twelve channel girders were tested to evaluate baseline moment capacity and behavior including the influence of aging and deterioration. The moment capacity of the channel girder specimens varied depending on their state of deterioration. Channel girders with exposed and corroded strands exhibited lower flexural capacity in comparison to channels with no visible corrosion damage. Damage was classified into three categories based on strand corrosion and measured moment capacity: low, medium, and high. The average experimental moment capacity of channel girders was as follows:

- 234 kip-ft, which is 23% higher than nominal moment capacity for channel girders with low damage.
- 179 kip-ft, which is 7% lower than nominal moment capacity for channel girders with medium damage.
- 143 kip-ft, which is 34% lower than the nominal moment capacity for channel girders with high damage.

This information may be helpful to engineers in evaluating the condition and capacity of skinny-leg channel girder bridges.

A strengthening scheme utilizing externally bolted aluminum structural shapes was developed and evaluated for channel girders. Aluminum was chosen for constructability reasons as it is light in weight, readily available, easy to handle in the field, and its corrosion resistance offers durability benefits. Aluminum channel sections were attached to skinny leg channel girders using epoxy or bolting. Aluminum reinforcement improved the flexural capacity by 9% to 33% relative to baseline girders. The specimen with aluminum channels attached by bolts along the entire span provided the best performance in terms of strength and ductility.

Laboratory and field tests were conducted to evaluate the effect of transverse post-tensioning (XPT) and latex-modified concrete (LMC) toppings on load distribution in skinny-leg channel bridges. By improving load distribution, truck loads are better ‘spread out’ and the load supported by individual channel girders is decreased. SC channel girder bridges were designed and built with steel tie rods that run transversely through the top flanges. The tie rods were removed, leaving ducts for installing post-tensioning reinforcement. Due to encouraging results in laboratory tests, XPT and LMC were evaluated on an out-of-service skinny leg channel girder bridge. Both concepts improved load distribution in the test bridge relative to the unmodified condition. For interior girders the retrofits improved load distribution by 15% to 29%, with improvements of 5% to 15% for exterior girders. It is estimated that similar retrofits could improve the load ratings of approximately 37 bridges to a satisfactory level.

In the final phase of the project, field tests were conducted to evaluate two concepts for retrofitting flat slab panel bridges. Both concepts were conducted from above as opposed to the more conventional approach of retrofitting from beneath the bridge. Retrofitting from above was pursued due to the relative ease of construction from above the bridge, which includes cost and time savings associated with scaffolding or other means of access associated with retrofitting or strengthening from below. The first concept tied adjacent panels together using carbon fiber ‘biscuits’, a technology that has been successfully deployed to tie components together in precast concrete parking garages. Biscuits are installed in grout-filled saw cuts made across adjacent panels. The intent of the biscuits is to improve load distribution. The second concept involved near-surface mounted (NSM) bars placed as negative moment reinforcement over the bent caps. The intent is to reduce moment demand by tying spans together as continuous members. The concept was demonstrated in the lab during a previous SCDOT project (SPR 752 – Safe and Cost-Effective Removal of Load Postings for South Carolina Bridges) with promising results. Field results indicated that the carbon fiber biscuits were relatively easy to deploy in comparison to the near surface mounted bars.

Contents

CHAPTER 1: INTRODUCTION

1.1 Problem Description

The transportation infrastructure in South Carolina includes many bridges that are load-posted due to structural considerations (e.g., outdated design loads, members whose capacity is difficult to assess), resulting in substantial costs to the public. Load-posted bridges have an adverse effect on travel and commerce in South Carolina. Cost-effective strengthening methods are required to mitigate these effects.

The South Carolina Department of Transportation is continually load rating its inventory of over 9,400 bridges. Precast flat slabs and skinny leg channel girders are problematic superstructure types. Many precast flat slab and channel bridges are understrength with respect to rating vehicles and therefore will require intervention in the form of posting, strengthening, or replacement. This project focuses on both laboratory and field trials of cost-effective strengthening methods for understrength precast flat slab and channel bridges.

The first phase of this project describes laboratory tests and field studies of precast-pretensioned channel girders and bridges. There are approximately 500 channel bridges throughout South Carolina, representing slightly more than 5% of the State's inventory. These bridges are 47 years old on average. The name comes from the cross-section shape that creates a channel along the span length. Two types of channels are common in South Carolina and are informally referred to as 'skinny leg' or 'wide leg' based on the width of the stems. Channel girder bridges typically have multiple simple spans of approximately 30 ft. and were designed using H15 loading. Most of the skinny leg channel bridges in South Carolina do not satisfy the load rating criteria for flexure (Figure 1.1).

The final phase of the project involved a field study to evaluate retrofits made to a precast flat slab bridge. The field study complements previous laboratory investigations (SPR 752) that focused on precast flat slabs. Cost-effective retrofits for flat slab bridges can have a significant impact as these bridges represent approximately 30% of the South Carolina bridge inventory.

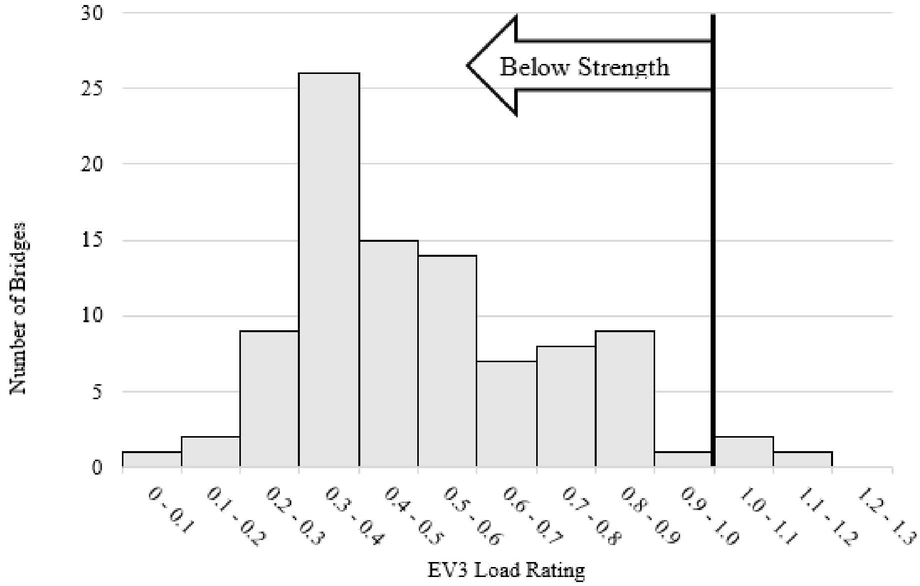

Figure 1.1 Load rating distribution for skinny leg girder bridges in South Carolina.

1.2 Goals and Objectives

The overarching goal is to reduce the number and severity of bridge load postings in South Carolina. The project identified, customized, implemented, and evaluated cost-effective strengthening strategies.

Specific objectives include:

- Benchmarking the flexural strength of prestressed concrete skinny leg channel girders through experimental testing.
- Evaluation of laboratory test results to determine factors affecting skinny leg channel flexural strength.
- Development of cost-effective strengthening strategies for both skinny leg channel and precast flat slab bridges.
- Field implementation and evaluation of the developed strengthening strategies.

CHAPTER 2: OVERVIEW OF GIRDER STRENGTHENING

Reinforced concrete (RC) bridges may require strengthening due to material deterioration, changes in use, accidents, and increased load demand. This section provides an overview of selected studies investigating strengthening methods.

Aidoo et al., 2006 examined a strengthening method for concrete bridge girders consisting of adhesively bonding carbon fiber-reinforced polymer (CFRP) on the bottom face. Three different CFRP systems were investigated: a) a conventional adhesive application (CAA), b) a near-surface mounted (NSM) method, and c) a hybrid carbon-glass FRP strip method utilizing a powder-actuated fastener (PAF) system (Figure 2.1). The test specimens were 33 in. deep, 37 in. wide, and 30 ft. long RC girders removed from a decommissioned bridge in Gaffney, SC. Eight specimens were tested, including one unstrengthened control specimen and two strengthened specimens for each type. For each strengthening type one specimen was tested under monotonic loading and the other under fatigue loading.

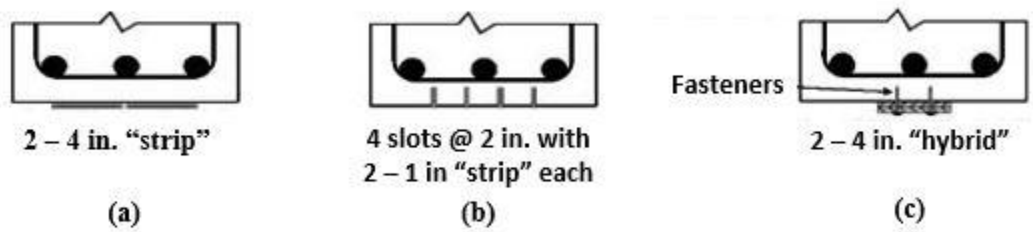

Figure 2.1 Strengthening methods used for RC girders: (a) CAA retrofit; (b) NSM retrofit; (c) PAF retrofit (Aidoo et al., 2006).

The primary mode of failure for monotonically loaded girders was crack-induced debonding. For specimens under repeat loading fatigue led to degradation of the CFRP to concrete bond. For the monotonic specimens CAA, NSM, and PAF, the ultimate load was increased by 4.5%, 5.6%, and 17%, respectively, compared to the unstrengthened control specimen. Compared to the control, ductility was 50% less, 13% greater, and 35% less for CAA, NSM, and PAF, respectively.

Yang et al. (2011) reported the utilization of externally bonded CFRP laminates as a repair technique for damaged concrete bridges. The first case was an exterior girder of a bridge impacted by an over height vehicle resulting in fracturing the entire web and bottom flange and severing one of the 44 prestressing strands (Figure 2.2a). Following the completion of concrete repairs, epoxy injection of cracks, and material curing one ply of CFRP U-wrap was attached to the web and bottom flange of the girder as shown in Figure 2.2b. After five years no signs of delamination or other CFRP composite deterioration were found (Figure 2.2c).

(a) (b) (c)

Figure 2.2 Bridge girder repair with externally bonded CFRP laminates: (a) impact-damaged beam; (b) continuous CFRP U-wrap after installation; (c) five years after repair (Yang et al. (2011).

The second case from Yang et al. (2011) was a prestressed concrete girder damaged by a truck impact and strengthened with externally bonded CFRP strips. Additionally, severed strands were spliced as part of the repair (Figure 2.3). The impact severed 25% of the strands; the calculated nominal moment capacity after the strands were severed was only 41% of the undamaged cross-section. The girder could be repaired to approximately 80% of its original capacity using only CFRP or only strand splicing. By utilizing strand splicing and CFRP the calculated capacity of the repaired girder was 95%.

(a) (b) (c)

Figure 2.3 (a) Impact-damaged beam; (b) splicing of strands; (c) placement of CFRP (Yang et al., 2011).

Aykac et al. (2013) investigated the flexural behavior of reinforced concrete (RC) beams strengthened with externally bonded steel plates. Thirteen full-scale RC beams (20 in. thick, 8 in. wide, and 15 ft. long) were tested with variables including plate thickness, plate anchoring using anchor bolts or collars, and perforated versus solid plates. One of the beams was also an unstrengthened control specimen. The primary goals were to understand if peeling of external plates could be prevented and if a plated beam could achieve ductile flexural behavior. Results showed that steel plates anchored by bolts or collars were an efficient approach to prevent early peeling failure and obtain appropriate ductility. Perforated plates enhanced the ductility of the beams relative to the solid plates.

Rasheed et al. (2017) conducted a study to validate the potential for employing Aluminum Alloy (AA) plates as an externally bonded strengthening material. The behavior of AA-strengthened beams was evaluated with and without CFRP sheets (U-wrap) acting as end anchorages. Ten RC beam specimens were tested. The plates were 79 and 118 mils thick, and both single and doublelayer U-wrap CFRP sheets were used as additional end anchorage. The strengthened beams showed an increase in flexural strength of 13% to 40%. End anchorages were observed to enhance the ductility of the strengthened beams to levels of ductility that were comparable to a control specimen.

Al-Osta et al. (2017) tested a method of strengthening RC beams using ultra-high-performance fiber-reinforced concrete (UHPFRC). The beams were 9 in. thick, 5.5 in. wide, and 5 ft. long. One beam served as a control specimen and the remaining beams were strengthened. The strengthening techniques increased the cracking load with respect to the control specimen. Addition of UHPFRC sometimes resulted in brittle failure and reduced ductility.

Distribution Factors

In addition to strengthening, improvements in lateral load distribution for bridges can be a useful means to increase load carrying capacity. In bridges with poor load distribution truck loads are primarily carried by the girders directly below the truck, whereas the load is spread to many girders in bridges having good load distribution (Figure 2.4).

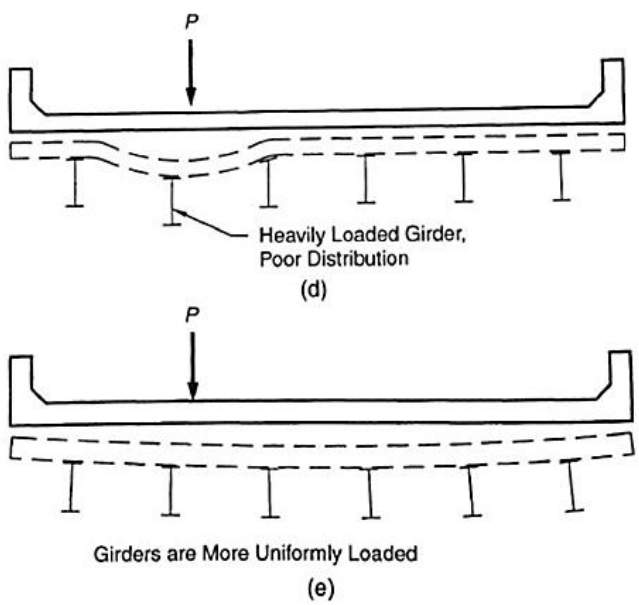

Fig 2.4 Conceptual description of load distribution (Baker and Puckett, 2007)

Distribution factors can be experimentally determined by measuring the structural response of girders under load. The distribution factor for girder i (DF_i) can be calculated as the displacement of girder i (δi) divided by the sum of all girder displacements, written as:

$$DF_i = \frac{\delta_i}{\sum_{i=1}^{i=n} \delta_i}$$

The distribution factor for a given girder represents the portion of the applied load that is carried by that girder.

Load distribution in a channel girder bridge near Liberty, SC was investigated experimentally by Eubanks, W. (2023). Based on measured strain data the distribution factors ranged from 0.37 to 0.44, depending on position of the load truck. A distribution factor of 0.50 is the theoretical limit for a girder distribution factor, meaning that the girder directly below the wheel lines is taking all the wheel load. The measured factors are near the theoretical maximum, which is consistent with poor lateral load distribution. Load rating factors can be improved by improving load distribution. As an example, a 20% improvement in lateral load distribution indicates that the load supported by a given girder is reduced by 20%.

CHAPTER 3: LABORATORY INVESTIGATION OF SKINNY LEG CHANNEL GIRDERS - BASELINE

3.1 Summary and Key Takeaways

- The average experimental flexural capacity was 6% higher than the calculated capacity based on design drawings.
- Capacity was consistent with the visually assessed condition of the girders.
- Girders with high damage exhibited flexural capacity 13% lower than the calculated capacity.

This chapter addresses baseline performance of skinny leg channel girders tested at the University of South Carolina (USC) and Clemson University (CU). The testing provided data for unrepaired skinny leg channels for comparison to strengthened channels (addressed in later chapters).

3.2 Test Methods and Materials

The channel girders tested were originally used in 30 ft. span bridges constructed in the 1950's and 60's. They were then stored in SCDOT facilities following approximately three decades of service life. Design dimensions and reinforcement details of the channel girders are shown in Figure 3.1, which are based on drawings provided by SCDOT. According to the design, typical longitudinal reinforcement consists of No. 3 bars evenly spaced in the top flange and ten 3/8 in. prestressing strands in the webs (Figure 3.1). Prestressing strands, except the bottom strands, were harped at midspan. The harped strands were prestressed to 13,450 lbs. prior to harping. The bottom strands were prestressed to 14,000 lbs. Transverse reinforcement consists of No. 4 bars spaced at 12 in. on center in the flanges and No. 4 stirrups spaced at 12 in. on center extending into the stems. The specified compressive strength (f'_c) of concrete was 5,000 psi. The specified yield strength (f_y) was 40,000 psi for the deformed steel bars and the prestressing strands were Grade 250. The plans also show diaphragms at each end; however, diaphragms were not present for some of the test specimens.

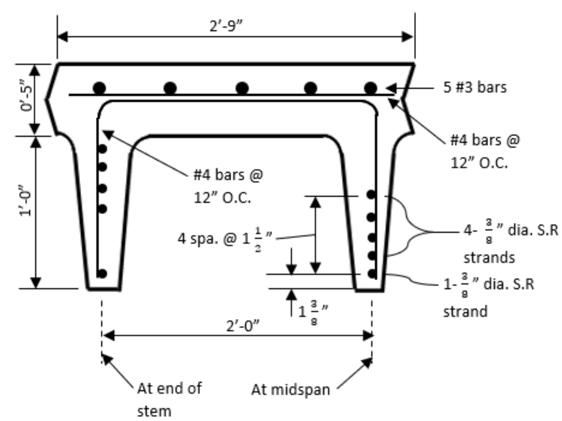

Figure 3.1 Cross section of a skinny leg channel girder.

Figure 3.2 is a schematic of the test setup. The channels spanned 27 ft. between support centerlines. Load was applied through two symmetric load points placed 10 ft. 6 in. from the supports. The test setup included neoprene bearing pads at each support, creating what is assumed to be a simply supported bearing condition. Steel members spread the load from the actuator to the channel, with neoprene bearing pads at contacts with the channel. These points of contact are designed to rest directly over the channel legs (also referred to as channel ‘stems’). The load cell used to record applied load is situated at the center line of the spreader beam. String potentiometers were used to measure vertical deflection at midspan. Load was applied using a hydraulic cylinder. Computer data acquisition systems were used to continuously record data. At CU, load was recorded using a pressure gauge in the hydraulic line; otherwise, the setup was the same at USC and CU. Figure 3.3 provides photographs of representative tests.

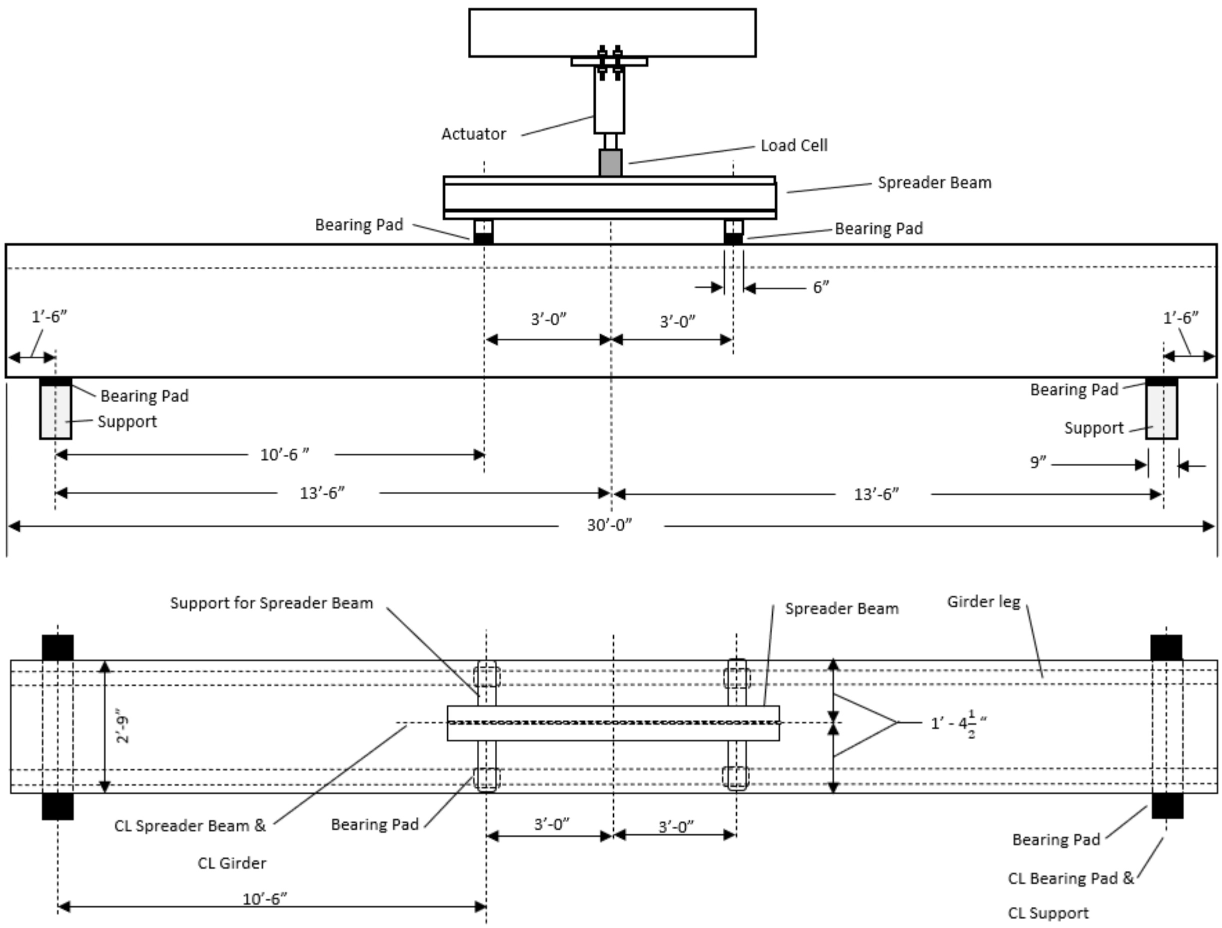

Figure 3.2 Elevation (top) and plan view (bottom) of skinny leg channel girder test setup.

Figure 3.3 Skinny leg channel girder test setup; (left) University of South Carolina, (right) Clemson University.

3.3 Results and Discussion

Table 3.1 summarizes the test results for the baseline channels. The average experimental moment capacity was 201 kip-ft., or 6% greater than the calculated nominal capacity of 189 kip-ft. CU test #6 is omitted from the average due to severe damage prior to testing, having lost all strands in one of the legs. Channels with this level of damage are likely beyond repair; hence, CU #6 was primarily tested as an academic exercise. The average experimental capacity and ductility decreased as the level of damage increased. Ductility in this case is evaluated from the deflection corresponding to the peak experimental moment.

Table 3.1 Test information and summary of results.

Test	Lab	Source	Asphalt (in.)	Diaphrag m present?	Moment from wearing surface (kip-ft.)	Max. moment in load test* (kip-ft.)	Deflection at max. moment (in.)	Damage state
1	CU	Fork Shoals	-	No	-	245	10.2	Low
2	CU	Fork Shoals	-	No	-	252	14.5	Low
3	CU	Fork Shoals	-	No	-	244	10.5	Low
**4	CU	Fork Shoals	-	Yes	-	183	7.70	Medium
5	CU	Fork Shoals	-	Yes	-	165	3.40	High
6	CU	Fork Shoals	-	Yes	-	97	4.30	High
1	USC	Saluda Yard	2	Yes	5.5	172	4.40	Medium
2	USC	Saluda Yard	2	Yes	4.6	184	4.40	Medium
3	USC	Saluda Yard	-	Yes	-	166	3.30	High
4	USC	Saluda Yard	-	Yes	-	227	11.0	Low
5	USC	Saluda Yard	-	Yes	-	202	5.00	Low
6	USC	Saluda Yard	-	Yes	-	177	6.60	Medium
Average						202	7.40	All***
						234	10.2	Low
						179	5.80	Medium
						166	3.40	High***

** Includes moment from self-weight (22.3 kip-ft), wearing service (if present) and applied load.*
*** Load points 10 ft. from support*
**** CU #6 not included due to severe damage prior to testing*

Figure 3.4 provides plots of applied moment versus vertical deflection for tests of unstrengthened channel specimens. The data include the contribution of the dead weight of the channel (including the wearing surface where applicable) and the applied load. The total dead load moment at mid-span was approximately 25 kip-ft. The response of the 12 channels was effectively linear and elastic up to a total moment of 75 kip-ft. The channels exhibited nonlinear behavior and continuous reduction in stiffness thereafter, without a well-defined yield point, as is typical of prestressed concrete members. Peak moment for each channel was controlled by strand rupture.

The tested capacity of the baseline channels was compared to the calculated capacity which was estimated based on information from SCDOT blueprints and the calculation process prescribed in AASHTO LRFD, (2017). The calculated capacity is indicated in Figure 3.4 with two horizontal dotted lines, one assuming nine working strands (175 kip-ft.) and one assuming 10 working strands (189 kip-ft.). The moment capacity for seven of the 12 specimens was less than the calculated capacity of specimens with ten strands (189 kip-ft.). This result is consistent with the observation that flexural capacity had been affected by damage. Four tests are shown to be well above the calculated capacity; these channels had intact strands and possibly higher than specified material properties.

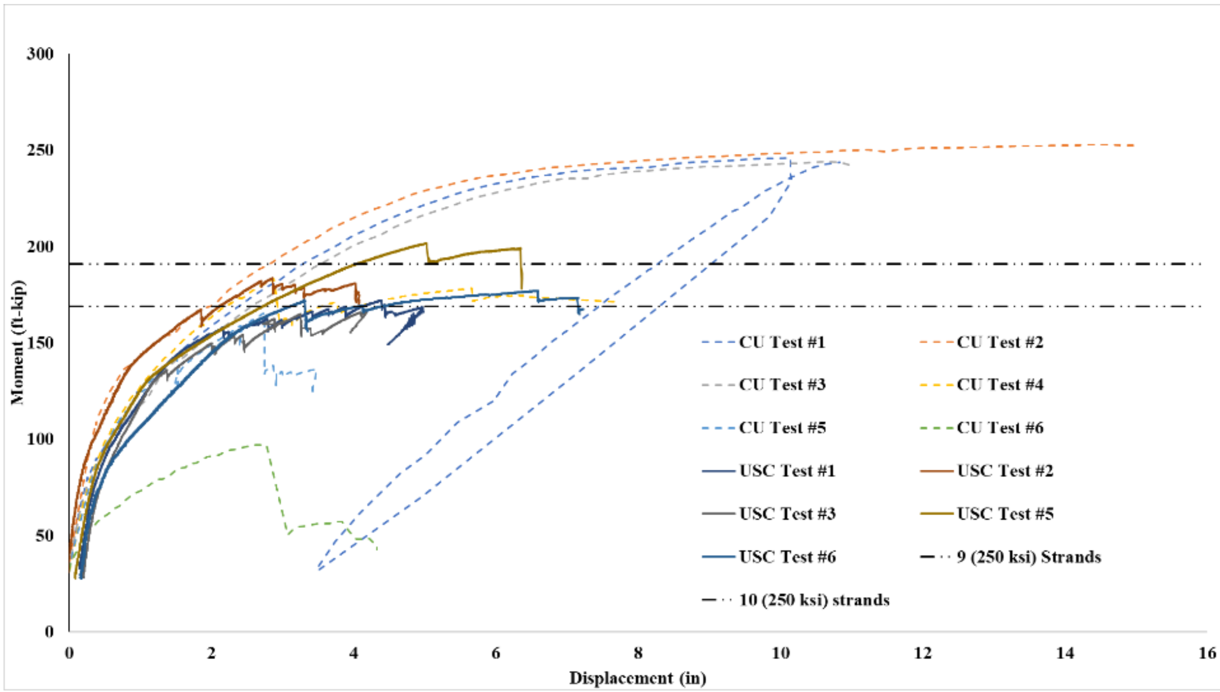

Figure 3.4 Experimental moment-displacement response of baseline channels.

Behavior at or near failure included strand yielding and rupture preceded by flexural cracking in the maximum moment region. An effort was made to correlate visually evaluated channel condition (amount of concrete cracking and spalling, strand corrosion) to tested capacity (Table 3.2; Figures 3.5 and 3.6). The damage level in each channel was characterized as either low, medium, or high. As expected, correlation was found with the strongest girders having the least damage.

Figure 3.5 Flexural cracking and strand rupture near midspan.

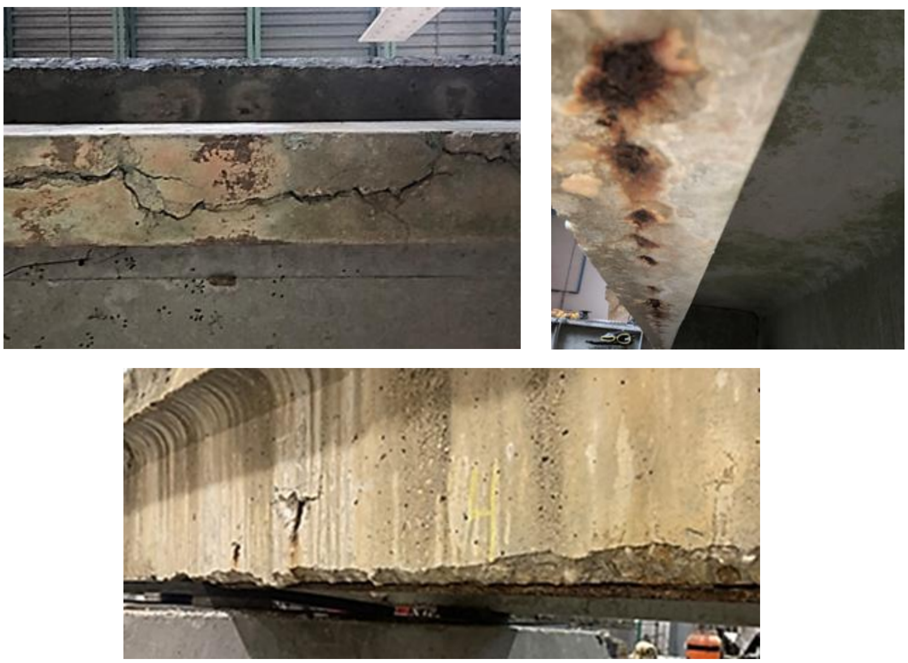

Figure 3.6 Evidence of spalling (top left), cracking (top right), and section loss (bottom).

Table 3.2 Damage categories and associated strand condition.

Classification	Strand Condition	Experimental Moment Capacity (kip-ft.)	Assumed Number of Working Strands	% Capacity Reduction	Strand Condition
Low Damage	Little to no evidence of corrosion	⩾ 189	10	0%	
Medium Damage	Evidence of corrosion in multiple locations or along a significant length of strand(s)	188 to 169	10 to 9	0% to 13%	
High Damage	One or multiple strands rendered useless due to several feet of severe corrosion of one or multiple strands, section loss clearly evident and significant	< 169	< 9	> 13%	

3.4 Conclusions

The load-deflection response can be characterized by three stages: 1) pre-cracking with a linear-elastic response, 2) a non-linear phase with no obvious yield point, and 3) a post-yielding phase with strand rupture. Strand rupture precipitated failure in all baseline channel tests.

The average experimental moment capacity was 202 kip-ft. which is 6% higher than the calculated moment capacity based on design drawings. Relative to the calculated capacity, channels with low, medium, and high levels of damage had average experimental capacities that were 23% higher, 7% lower, and 13% lower than calculated capacities.

Channel capacity was significantly affected by the condition of the girder. Many channels contained visibly corroded strands prior to testing, with spalling, cracking, and section loss at or near the soffits. Damage in the form of exposed and corroded strands corresponded to a significant reduction in experimental capacity and ductility.

Channels from CU tests #1-3 had the highest experimental capacities in the test program. These channels exhibited low damage, which contributed to the above-average capacities. It is possible that these channels had material properties higher than specified in the SCDOT documents.

CHAPTER 4: LABORATORY TESTS OF CHANNEL GIRDERS STRENGTHENED WITH ALUMINUM SHAPES

4.1 Summary and Key Takeaways

- With the goal of improving flexural capacity, aluminum shapes were attached to skinny-leg channel girders using bolts and/or epoxy-based adhesive.
- Aluminum was chosen due to its light weight and corrosion resistance.
- The method of attaching the aluminum affected the level of improvement. Bolted connections performed better than epoxy bonding.
- An increase in capacity of up to 33% was observed relative to comparable baseline channels.

4.2 Introduction

Aluminum alloys (AA) have desirable properties for external strengthening. This chapter explores the feasibility of using AA channel shapes as external reinforcement for skinny leg channel girders. Three specimens were modified by external bonding and/or mechanical bolting of AA shapes to the channel legs (Figure 4.1). Each specimen was labeled as follows: SE for epoxy-bonded, SB for aluminum shapes bolted to the legs without epoxy, and SEB for both bolted and epoxy-bonded aluminum shapes. Referring to the damage characterization scale from Chapter 3, specimen SE was in the medium damage state while SEB and SB had low damage. The bolting patterns for SB and SEB varied as shown in Figure 4.1.

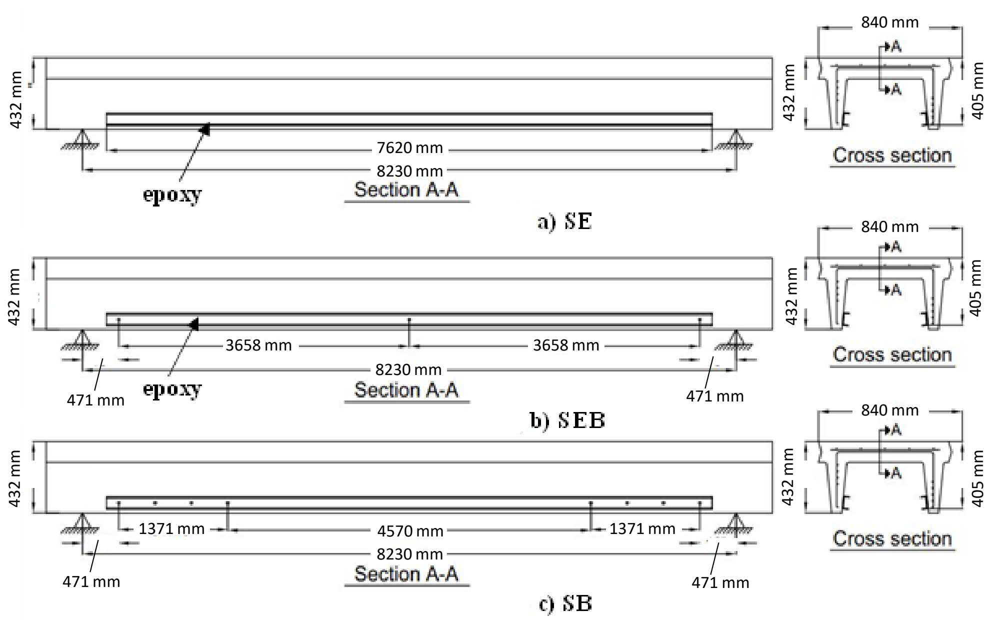

Figure 4.1 Strengthening schemes: a) SE; b) SEB; and c) SB (1 in. = 25.4 mm).

4.3 Test Methods and Materials

Each specimen was modified by attaching two 25 ft. long AA shapes to the webs. The AA shapes were designated as CH3 × 258. The shape is approximately 3 in. tall with a 0.258 in. thick web with flanges approximately 1.5 in. wide and 0.2 in. thick. The material was 6061-T6 aluminum.

SikaDur-30 epoxy adhesive was used to attach the AA shapes to specimen SE. Surface preparation and epoxy application followed guidelines provided by the manufacturer. The concrete was roughened by needle scaling to achieve a minimum concrete surface profile of 3 (Figure 4.2). The AA surface was roughened using 400-grit sandpaper. Epoxy adhesive was applied to both concrete and AA surfaces and the shapes were clamped in place as the epoxy cured. This specimen was load tested seven days after the AA shapes were attached.

Figure 4.2 (left) surface preparation by needle scaler; (right) aluminum shapes in place.

AA shapes were attached to specimen SEB using the same materials and procedure as described for specimen SE. In addition, the shapes were bolted to the concrete at the ends and midspan using 5/8 in. diameter 6061 aluminum threaded rods (Figure 4.3). The rods were installed through ¾ in. diameter holes drilled through the beam webs. Ground penetrating radar was used to locate the prestressing strands and to coordinate the drilling locations. Holes were cleaned with an air compressor before installing the aluminum rod. The aluminum threaded rods were secured using aluminum hex nuts which were tightened using a wrench.

Figure 4.3 Aluminum channels bonded and through-bolted with aluminum threaded rods.

For specimen SB, only mechanical attachments were used to connect the AA shapes (epoxy was not used). Each end was attached using four 5/8 in. diameter ASTM 192 Grade B7 steel threaded rods. The intent of switching from aluminum rods (specimen SEB) to steel rods (SB) was to increase the capacity of the bolted attachments. The size and quantity of steel rods were selected with the intent to approach the yield capacity of the AA shape prior to failure. The locations and spacing of the rods are shown in Figure 4.1 and Figure 4.4. In field applications, care should be taken to mitigate the possibility of galvanic corrosion resulting from the combination of steel bolts and aluminum. The use of sealants, tapes, and/or gaskets is recommended for consideration.

Figure 4.4 Aluminum channels through-bolted with steel threaded rods.

4.4 Results and Discussion

The experimental moment and midspan vertical displacement of the strengthened channel girders are shown in Figure 4.5. The moment includes both self-weight and applied load. Two stages characterize the general behavior observed in the figure. The first stage is characterized by pre-cracking, exhibiting a linear moment-displacement response, followed by a non-linear phase with no discernible yield point. Response of the specimens varied at moments greater than approximately 120 kip-ft. As expected, specimens SE and SEB with epoxy-bonded AA had greater stiffness than specimen SB for which the aluminum shapes were only mechanically attached.

The peak experimental moment for specimen SE corresponded to the AA shape debonding along the length of the beam (4.6 a). Failure of SEB was similar but also included shearing of the threaded aluminum rods (Figure 4.6 b). Debonding in SE and SEB occurred abruptly. Specimen SEB supported a larger moment. The difference in capacity may be partially attributed to the condition of the girders, as SE was in poor condition, whereas SEB was in good condition. It is reasoned that the epoxy and mechanical attachments in specimen SEB acted in such a way that their combined effect was not additive, meaning the epoxy failed first and then the load was transferred to the aluminum threaded rods. The failure mode was shearing of the aluminum rods, indicating that the rods were somewhat effective for increasing flexural capacity.

Specimen SB exhibited the highest experimental moment and showed the greatest ductility among the strengthened specimens. The failure mode of specimen SB was concrete splitting at the steel end bolts (Figure 4.6 c). Results from all three specimens are summarized in Table 4.1. These results pertain to the strengthening configurations presented in Figure 4.1, and may change depending on bolt type (material, size), number, and spacing. For example, the performance of the SB system might further increase if the design is optimized.

Table 4.1 Test results for AA strengthened channel girders.

Specimen	**Calc. moment capacity, (kip-ft)**	**Exp. moment capacity, (kip-ft)**	**Exp./Calc. ratio**	**Displacement at peak exp. moment (in.)**	**Condition rating of beam before testing**	**Failure mode**
SE	294	190	0.65	1.8	Poor	Debonding
SEB	294	246	0.84	2.7	Good	End bolt rupture
SB	294	285	0.97	8.0	Good	Concrete splitting at end bolt

Figure 4.5 includes dashed horizontal lines showing the calculated moment capacity of unmodified and AA shape modified skinny-leg channel girders. The capacities were calculated in accordance with the AASHTO LRFD (2017) and using specified material properties and dimensions. Strain compatibility was assumed between the girders and AA shapes. Additionally, it was assumed that the aluminum yielded when the beam reached its moment capacity. With these assumptions, the calculated capacity of the AA-strengthened beams was 294 kip-ft, which is a 54% increase in calculated capacity relative to the baseline of 189 kip-ft.

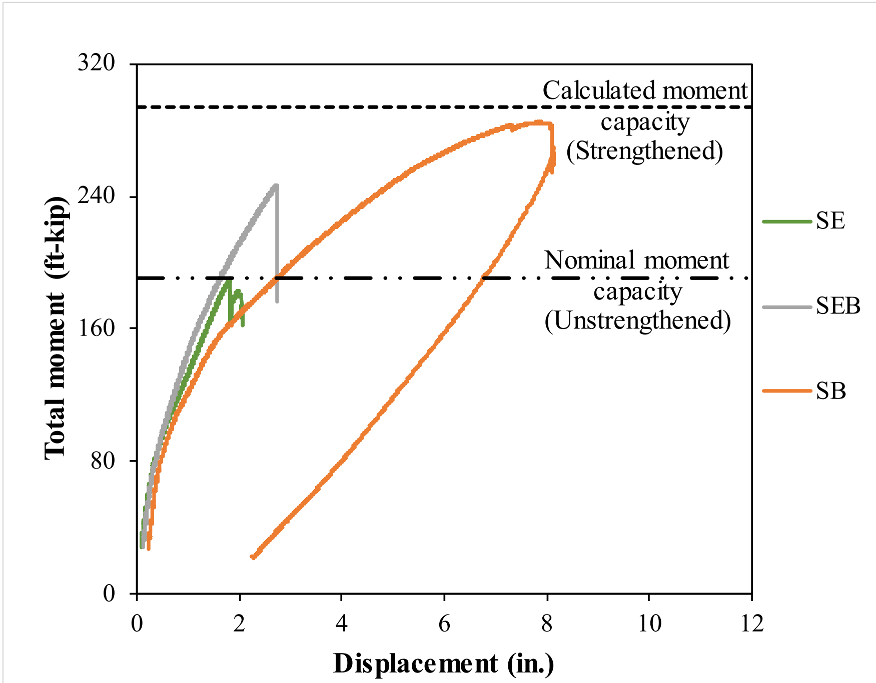

Figure 4.5 Moment versus midspan vertical displacement for the strengthened girders.

a) Debonding of the AA channels for specimen SE.

b) End bolt rupture for Specimen SEB.

c) Concrete splitting at end bolt for Specimen SB.

Figure 4.6 Failure modes for strengthened girders.

Strains in the AA shapes were monitored during testing to better understand the degree to which the shapes were engaged. Strains at failure in the AA shapes were in the range of 0.0030 and 0.0025 for specimens SEB and SB, respectively. The experimental strains were lower than the specified yield strain of 0.0040, however specimen SB approached this value more closely. While it is not imperative that the AA shapes be fully developed it is a convenient target for design purposes. As the bolting requires time and resources, if the yielding of the shapes as a failure mode is desired it may be considered to reduce the cross-sectional area of the AA shapes, either locally through perforations or by selecting shapes with lower cross-sectional area.

The experimental capacity of specimens SE and SEB was 65% and 84% of the calculated moment capacity assuming full development of the AA shapes. For specimen SEB the experimental capacity approached 97%. Additional bolted attachments would have better engaged the AA shapes for this specimen, though at the cost of increased effort in the field.

Another way to view the results is to compare the AA strengthening to baseline girders having similar levels of damage. Girders tested at USC demonstrated flexural capacities of 202 and 227 kip-ft. (for USC specimens #4 and #5, respectively), resulting in an average value of 215 kip-ft. The capacity of specimen SB exceeded this value by 33%.

4.5 Conclusions

Based on the experimental findings the following conclusions are drawn:

- Each of the AA-shape strengthened girders had higher experimental capacities and lower displacements than comparable unstrengthened baseline specimens. Performance varied according to the method used to attach the AA shapes to the channel girders.
- For epoxy-bonded (SE) and bonded/bolted (SEB) specimens, abrupt failures occurred due to debonding. Given the abrupt failures and modest strength gains demonstrated, the epoxy-bonded attachment methods used are not recommended.
- Bolting the AA shapes to the channel girders was a more convenient method in terms of practicality and ease of installation; it also resulted in the highest increase in moment capacity. It is recommended that steel bolts be utilized in field applications due to superior strength and ductility in comparison to aluminum. Bolts are recommended over threaded rods to minimize stress concentrations in the potential plane of splitting. Concrete splitting was the observed failure mode for specimen SB, which may be delayed or avoided through the use of larger diameter bolts or other means. However, the complications with larger diameter bolts including the potential for drilling through existing prestressing strands should be considered.

CHAPTER 5: LABORATORY TESTING OF LATEX MODIFIED CONCRETE (LMC) OVERLAYS AND TRANSVERSE POST-TENSIONING (XPT) TO IMPROVE LOAD DISTRIBUTION

5.1 Key Takeaways

- Laboratory testing demonstrated that transverse post-tensioning and latex-modified concrete overlays can improve load distribution between skinny-leg channel girders.
- Based on encouraging test results, both approaches warranted subsequent field testing (presented in Chapter 6).

5.2 Introduction

Three skinny leg channel girders were obtained from an SCDOT salvage yard in Saluda, SC. The girders were previously used in a bridge(s); however, the location, construction date, and salvage date are not known. The salvaged channels were positioned to form a three-channel system, which served as the test specimen for investigating the effects of transverse post-tensioning (XPT) and a latex-modified concrete (LMC) overlay on load distribution (Figure 5.1). As load was applied to one of the channels displacements were measured for each channel and used to evaluate the degree of load distribution through the system. Additional details may be found in the theses of Eubanks (2023) and Dodd (2023).

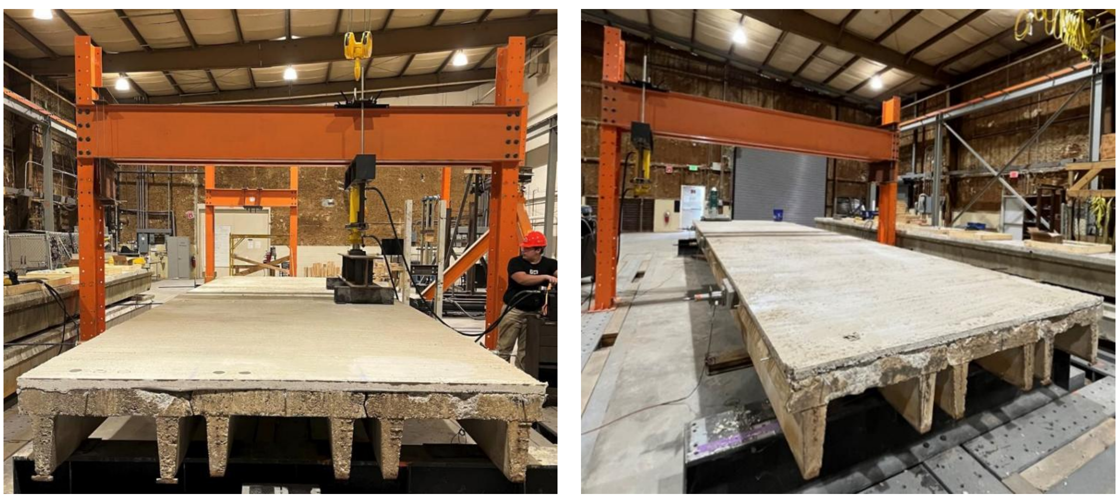

Figure 5.1 Two views of the three-channel girder system after LMC overlay was placed.

5.3 Test Method and Materials

Transverse Post-Tensioning

Original details for skinny-leg channel girder bridges included three transverse steel tie rods run through ducts cast into the flanges at approximately the quarter points of the span length. The steel tie rods were absent from the test specimens, allowing the ducts to be utilized for the installation of 0.6 in. diameter lo-lax strands (Figures 5.2 and 5.3).

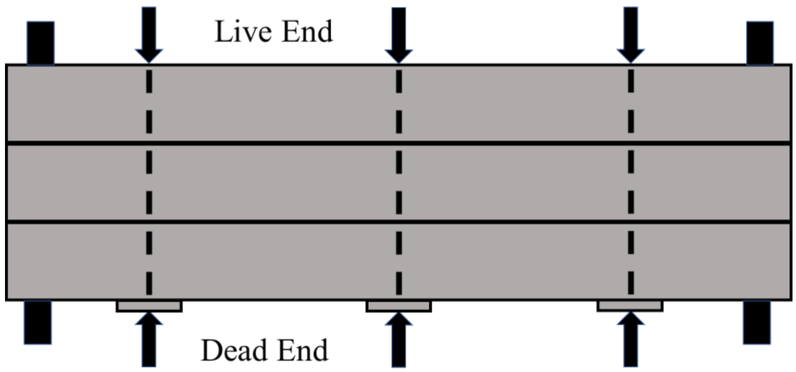

Figure 5.2 Plan view showing XPT locations.

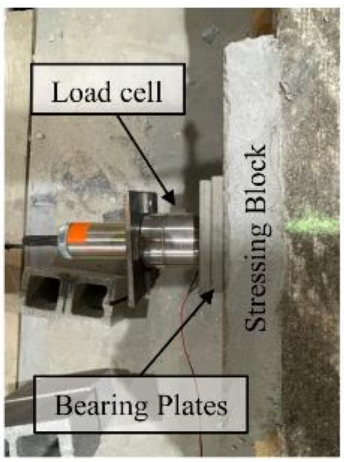

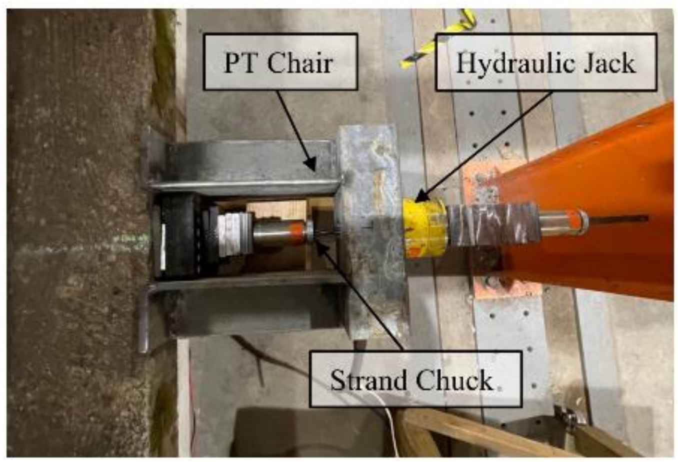

Figure 5.3 XPT installation: dead end (left) and live end (right).

Latex Modified Concrete Overlay

A 2 in. thick LMC overlay was placed on the three girder system. The surface of the girders was prepared with a 3,000 psi pressure washer several days prior to placing the overlay. Formwork consisted of wood boards installed at the edges of the three-channel system. The LMC was mixed in a batch mixer and then placed on the girder system using a forklift and bucket (Figure 5.4). The LMC mix followed the proportions in Table 5.1 which adhered to SCDOT specifications. The mix used a rapid-set cement.

Samples of the mix had 28-day compressive strength of 5,410 psi. In comparison, the LMC mix used in field trials (Chapter 6) had a 28-day strength of 4,120 psi. The variation in compressive strength is attributed to the different mix designs. For example, the mix from the lab tests (Table 5.1) used a rapid-set cement, whereas the field mix used Type IL.

The direct tension bond strength at 28 days ranged from 55 to 180 psi, with a mean of approximately 130 psi. Previous research on LMC reported tensile bond strengths ranging from just under 100 psi to over 400 psi (Sprinkel, 1992). This wide range of bond strength illustrates the potential variability in bond strength of LMC overlays.

Table 5.1 Mix proportions (per 80 lb. bag of cement).

Material	Material Amount (lb)
Rapid Set Cement	80
Latex Modifier	25.3
Natural Sand	175
#789 Washed Stone	151
Water	18.8

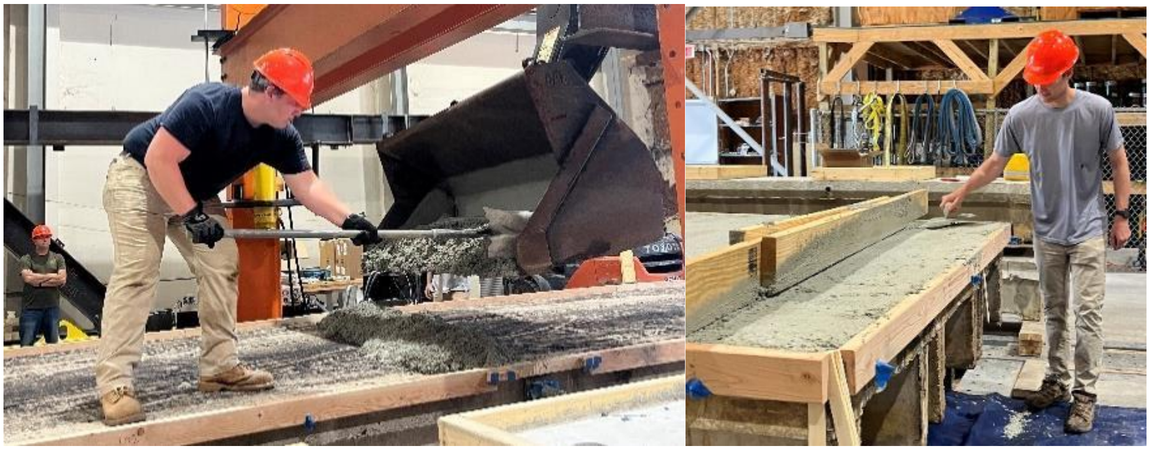

Figure 5.4 Placement (left) and finishing (right) of LMC overlay.

5.4 Test Parameters and Setup

Table 5.2 summarizes the test program. Phase one investigated load distribution under mimicked field conditions, i.e., minimal transverse force and no LMC overlay. Phase two investigated load distribution with only XPT. Phase three investigated the combined effects of LMC + XPT. The XPT was removed for phase four, which considered the load distribution of the system with LMC only. After phase four the individual channels were load tested.

Table 5.2 Parameters evaluated during testing.

<table>
<tr><th>Location of applied load</th><th>Mimicked field condition</th><th>XPT only</th><th>LMC + XPT</th><th>LMC Only</th></tr>
<tr><td>East Channel</td><td>Reported by Eubanks (2023)</td><td rowspan="3">Reported by Eubanks (2023)</td><td rowspan="3" colspan="2">Reported by Dodd (2023)</td></tr>
<tr><td>Center Channel</td><td rowspan="2">Not tested</td></tr>
<tr><td>West Channel</td></tr>
</table>

A schematic of the setup is shown in Figure 5.5. Six wire potentiometers were positioned at the midspan to measure vertical deflection. Load cells were used to monitor the force in each post-tensioning strand; however, only the center load cell recorded data continuously during loading. Load cells on the outer strands were periodically monitored during testing to ensure that the strand forces did not substantially change. Load was applied using a hydraulic jack and was continuously recorded using a pressure gage.

Load from the hydraulic jack was distributed to the top of the specimens through a steel spreader assembly, producing four different point loads. An elastomeric bearing pad was placed between the spreader assembly and LMC topping at each point load. The point loads extended transversely, ending across the top flange to points above the channel legs. In the longitudinal direction, they were offset from each side of midspan by 3 ft. resulting in a constant moment region at midspan. With the exception of the jack and spreader position the basic setup presented in Figure 5.5 was used for all tests. Three positions of the jack and spreader assembly were used: centered over the east, west, and center channels.

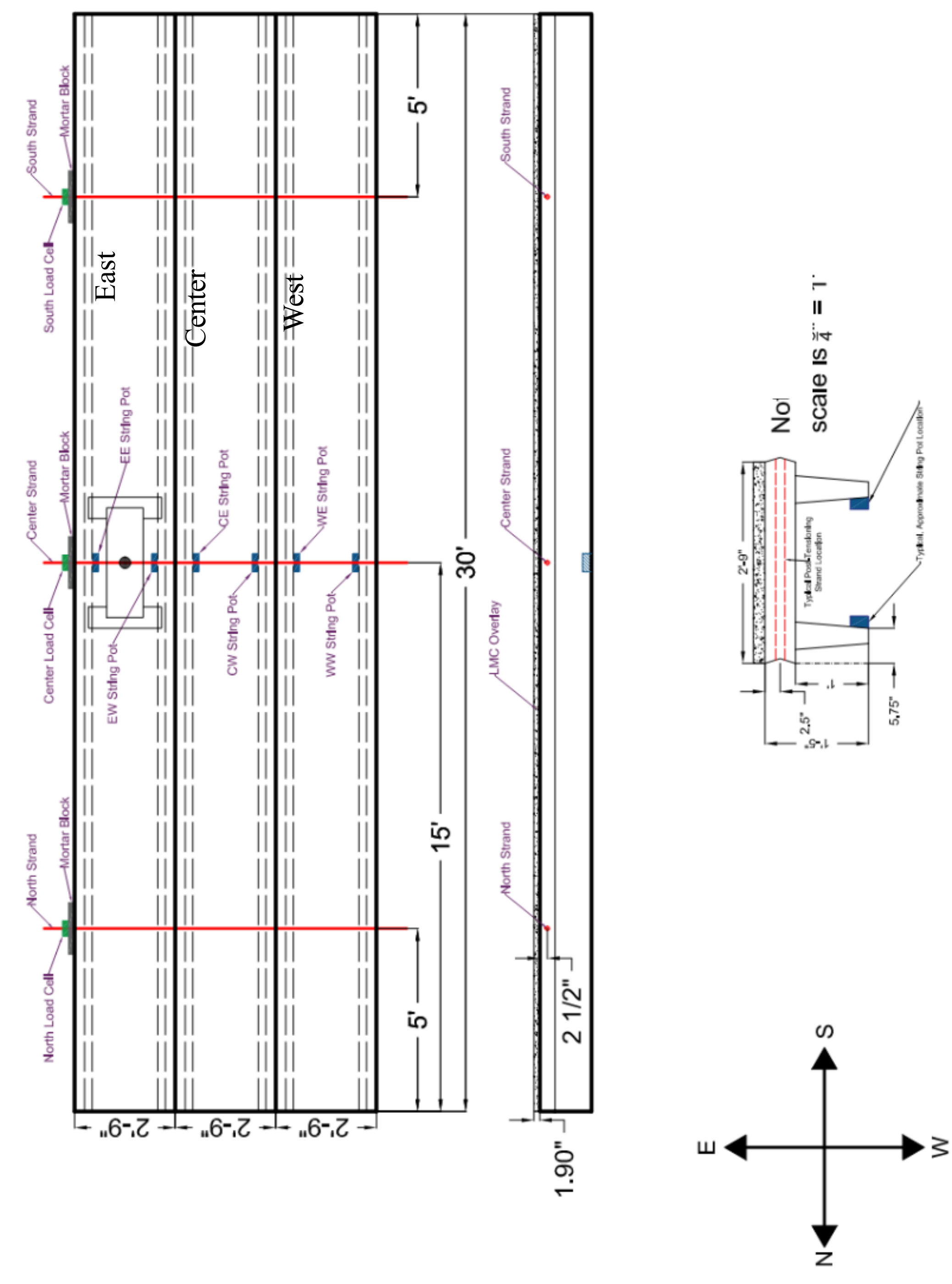

Figure 5.5 System instrumentation and layout.

To mimic service loading the maximum applied load to the system was 16 kips. This value was based on the HL-93 design truck (AASHTO 2020), which has a back axle weight of 32 kips, a wheel spacing of six feet, and a minimum axle spacing of fourteen feet. The value of 16 kips was chosen to simulate one wheel line from the back axle of the design truck loading a single girder. The front axle was not considered, as the axle spacing of an HL-93 truck is such that the front axle and back axle would not load the bridge at the same time.

5.5 Load Distribution Results and Discussion

Test results are presented in Figures 5.6 and 5.7. The 'Field Condition' results presented in Figure 5.6 were from a test intended to mimic field conditions of channel girders loosely held together by a tie rod. The tie rod was mimicked by placing and anchoring the strands but not tensioning them significantly. LMC had not yet been cast. In this condition, the load was applied to the eastern channel, which deflected significantly more than the other channels, indicating that a negligible degree of distribution was occurring. The full 16 kip service load was not applied in this condition to prevent cracking or other damage to the eastern channel. To facilitate comparison with the other conditions and higher load levels, displacement data in the figures were normalized by the applied load (deflections reported as in. per kip).

The load distribution improved significantly when the strands were post-tensioned and the LMC was placed. This can be observed by comparing the displacements from the field condition with those from the XPT and XPT + LMC conditions. These modifications engaged the center and western channels, causing them to displace as they attracted a portion of the applied load. The normalized displacement of the western channel with XPT was approximately half the normalized displacement from the field condition. The XPT + LMC case showed an even more substantial effect with approximately one-third of the normalized displacement. The high degree of load distribution in the XPT + LMC condition can also be observed in Figure 5.6, which shows that each channel had approximately the same displacement when the center channel was loaded.

The performance of the system was effectively symmetric about the center channel, meaning the results obtained when the load was applied above the western channel were similar to those presented in Figure 5.6 for the case when the eastern channel was loaded.

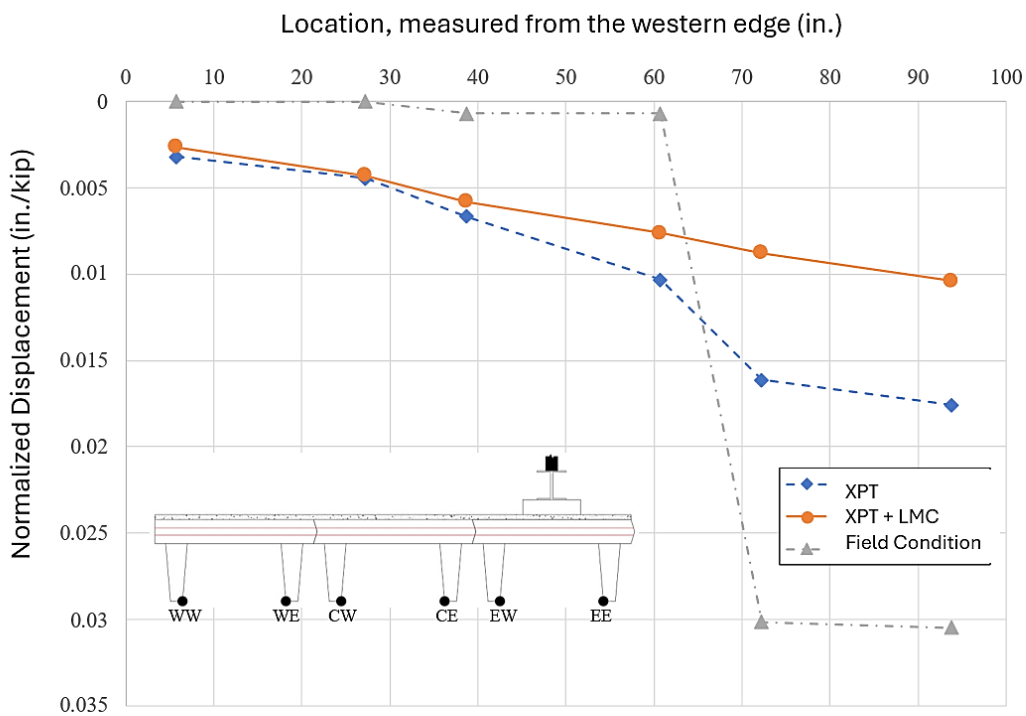

Figure 5.6 Normalized displacements, east girder loaded.

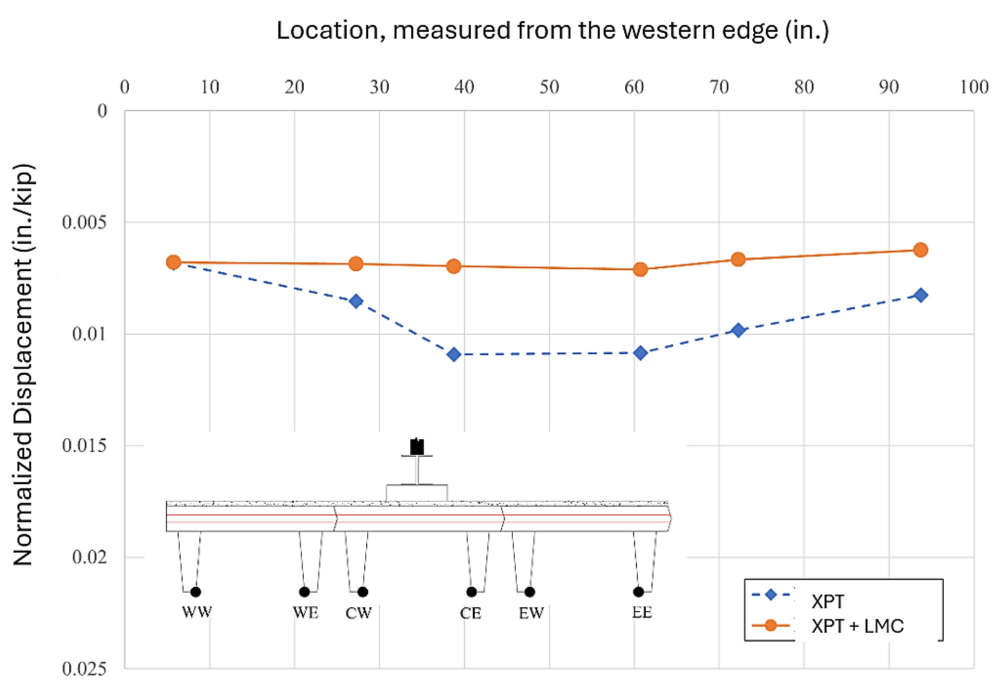

Figure 5.7 Normalized displacements, center girder loaded.

Test results were quantitatively compared by calculating the distribution factors for each combination of variables. The resulting distribution factors are shown in Table 5.3 with larger values indicating worse load distribution. For context, the distribution factors can be compared to a “perfect” value of 0.33, which would result if each channel carried the same amount of load and deflected equally. The application of transverse post-tensioning improved load distribution by 63% relative to the mimicked field condition. The improvement was 100% for the condition with transverse post-tensioning and LMC. The load distribution was highest (distribution factor, DF, lowest) when the load was applied above the center channel because the load could distribute in both directions. In contrast, load applied above the east and west channels only distributed load in one direction and had to travel through the center to reach the channel on the opposite side of the system.

Table 5.3 Experimental distribution factors (DF).

Load Location	Mimicked Field Condition	XPT	XPT + LMC
East channel	0.98	0.60	0.49
Center channel	Not tested	0.39	0.35
West channel		0.58	0.49

5.6 Conclusions

Transverse post-tensioning and latex-modified concrete overlays improved load distribution in laboratory tests of a system comprised of three adjacent skinny leg channel girders. When transverse post-tensioning was applied, load distribution improved by 63% relative to the baseline condition. The improvement was 100% when both transverse post-tensioning and the LMC overlay were present. Based on these promising results, both approaches were investigated through field trials of a skinny leg channel girder bridge.

CHAPTER 6: FIELD TESTS OF LMC AND XPT TO IMPROVE LOAD DISTRIBUTION

6.1 Summary and Key Takeaways

- Field tests were conducted to evaluate transverse post-tensioning (XPT) and latex-modified concrete (LMC) overlays to improve load distribution in a skinny leg channel girder bridge.
- Both XPT and LMC improved load distribution. The effects of both retrofits were similar, with load distribution improving by approximately 10% for truck paths near the edges and 20% for interior paths.
- Based on an evaluation of recent load rating data, these methods may justify the removal of load postings from one-third to one-half of skinny leg channel girder bridges.

6.2 Bridge Details and Test Methods

The field study utilized the Airport Road Bridge (ARB) in Greenwood, South Carolina. Details of the tests are reported by Waters (2024). The ARB consisted of multiple 30 ft. spans, with each span comprised of ten skinny leg channel girders (Figure 6.1). The bridge was closed and scheduled for replacement providing the opportunity to use it as a test bed for evaluating the retrofits. The span on the south end was used for testing.

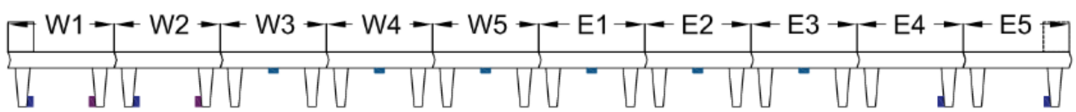

Figure 6.1 ARB cross-section and channel girder labels.

Multiple live-load field tests were conducted: one in September 2023 (as is, prior to modifications), two in November 2023 (without tie rods; with XPT), and two in May 2024 (with LMC overlay; both with and without XPT). The vertical deflection of each channel girder was measured as a load truck was driven slowly across the instrumented span at one of five different positions (Figure 6.1). Deflections were recorded for three separate 'runs' (truck crossings) for each truck position.

The as is test was performed with the bridge in its original condition, which included an asphalt overlay and one curb on the west side of the bridge. No modifications were made to the bridge before the as is test. Before the second test the tie rods were removed. The curb on the east side of the bridge was also removed to reduce the influence of a singular curb on the displacement response of the bridge. An XPT only test was conducted approximately two weeks after the post-tensioning installation, and an XPT and LMC test was performed approximately 36 days after the LMC overlay was placed.

Calibrated string potentiometers, or 'pots', were used to measure the vertical deflection of the bridge girders at midspan. To expedite data post processing all string pots used were labeled based on serial number and relative position from west to east. The pots were wirelessly connected to a data acquisition system and data was recorded at a rate of 20 readings/second. Load distribution was calculated from the experimental data using the approach described in Chapter 2.

The SCDOT provided the same truck (Figure 6.2) and driver for each load test, ensuring consistency across all tests. The truck was loaded to approximately the same weight for each test using gravel from a nearby quarry. The front and back axle weights were approximately 10 and 35 kips, respectively.

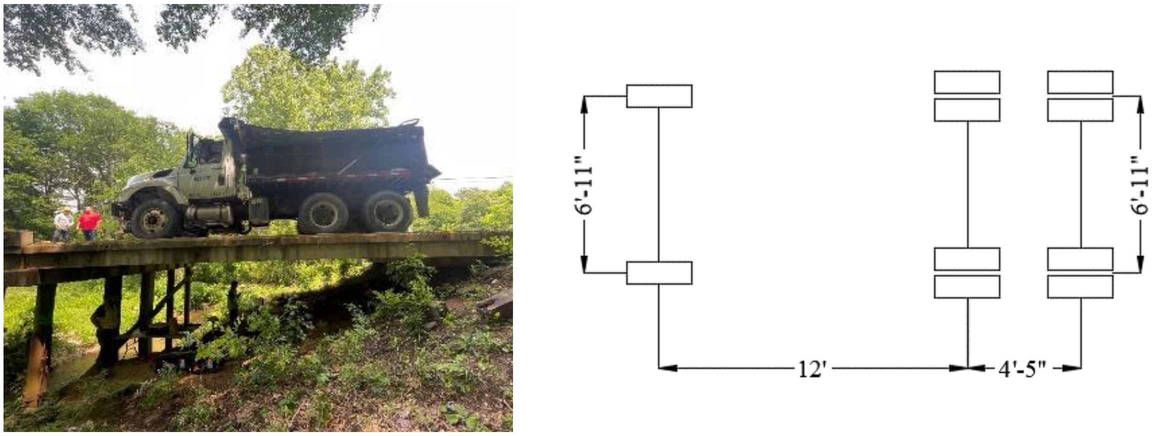

Figure 6.2 Photo (left) and dimensions (right) of load truck.

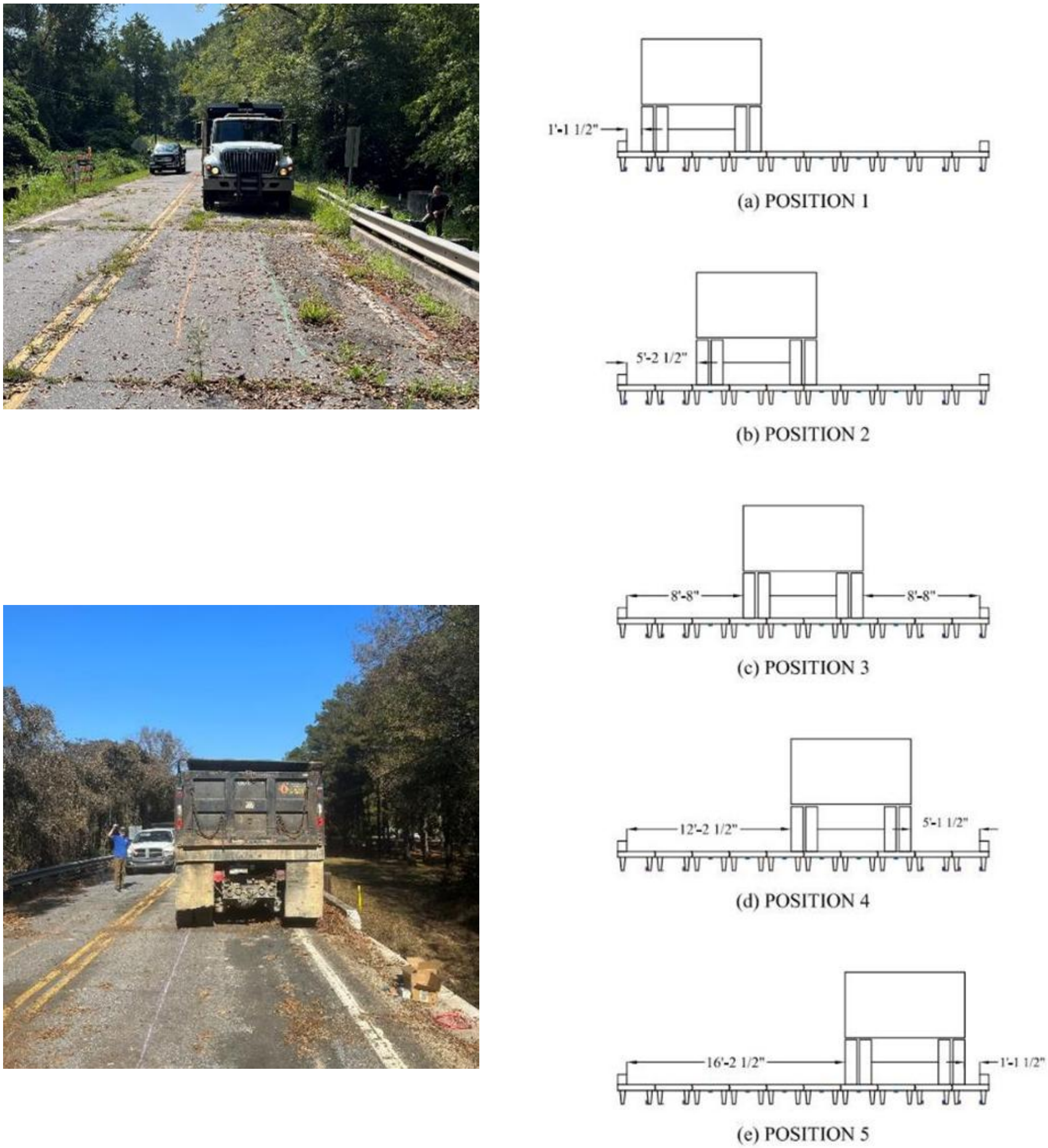

Figure 6.3 Truck crossing photos (left) and positions (right).

6.3 Retrofit Materials and Installation

After completing the 'as is' test the existing tie rods were removed and the bridge was retested. Before the third test, post-tensioning strands were installed through the three existing transverse holes that had been cleared by removing the tie rods. Prestressing strands (Grade 270 and 0.6 in. diameter) were delivered to the ARB site and cut to size, extending beyond the exterior girders by approximately 2 to 3 ft. A single post-tensioning strand was installed in each of the three tie-rod ducts. The dead end, or the end of the strand anchored to the bridge, was located on the east side of the bridge. Due to the short time frame and the absence of traffic on the bridge, no specific measures were taken to protect the strands from the elements. In practice, durability would be a consideration when selecting and designing the post-tensioning system.

A load cell was placed on the strand at midspan to monitor the force in the strand during tensioning, during subsequent live load testing, and at intervals between the tests. The anchorage, stressing equipment, and stressing procedure followed the lab testing described in Chapter 5. The strands were initially stressed to almost 30 kips. The force reduced to approximately 25 kips within a few weeks and 20 kips before removal at the end of testing. For the bridge geometry and strand properties, approximately 0.5 in. of strand shortening would have been required to achieve a 10 kip loss of prestress. While the causes of the prestress loss are not known, likely causes include settlement of the anchorages, relaxation of the strands, and incremental closure of the joint between channels. Any debris in the gap may have been crushed due to the load tests and movement from daily thermal cycles. Scraping off the asphalt and high-pressure water cleaning, conducted ahead of LMC placement, could have also contributed to gap closure, shortening of the post-tension strands, and reduction in force.

To prepare the bridge for LMC placement the asphalt overlay, which was approximately 5 in. thick, was scraped off using a backhoe. Asphalt removal was completed in approximately 3 hours. Before the LMC placement debris was removed from the bridge deck using a leaf blower, and the top surface and joints were cleaned using a pressure washer. The LMC provider typically recommends a minimum of 7,500 psi for waterblast cleaning; however, to evaluate the possibility of using a less aggressive approach, a 3,200 psi pressure washer was used. Pressure washing thoroughly cleaned the surface and removed debris from the joints (Figure 6.4). The remaining gaps in the joints were filled with mortar prior to placement of the LMC.

Wood strips were installed along the edges of the bridge as formwork for the LMC. The LMC was cast directly against the remaining asphalt topping at the abutment and the adjacent span.

 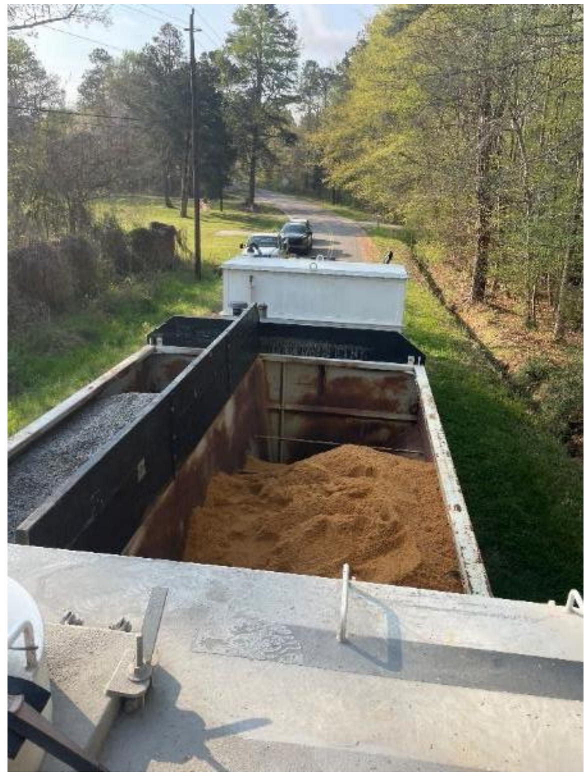

Figure 6.4 Pressure washing the surface and joints (left); LMC materials (right).

The LMC overlay was mixed and placed with the help of Modified Concrete Suppliers, LLC (MCS), which provided the volumetric mixer, water, cement, and latex admixture. MCS also assisted with the mix design (Table 6.1) and aggregate selection. The materials were combined and the LMC was prepared in a mobile volumetric mixer.

Table 6.1 LMC overlay mix design.

Material	Volume (cu ft)
Type 1L Cement	3.35
FA-10 Natural Sand	9.52
#789 Washed Stone	7.48
Latex	3.30
Water	2.00
Air	1.35
Total	27.0

The concrete surface was wetted immediately prior to placing the LMC. Once the placement began a mixing auger on a swivel allowed for ease of placement. The LMC was placed first on the west half of the bridge, and as it was poured, a screed board was used to level the surface. This was followed by using a hand trowel where needed and finishing with a bull float across the entire surface. Once the west side was complete the formwork placed down the center of the bridge was removed and the process was repeated on the east side. A burlap blanket was laid to cover the LMC overlay and water was sprayed to moisten the blanket to promote curing. The burlap blanket remained moist during the first 48 hours of curing before being removed several days later. Cylinders were made for subsequent compression testing.

6.4 Results and Discussion

Distribution factors recommended by WSP (Table 6.2) from a report for similar channel girder bridges provide a basis for comparison to the experimental results. The recommended distribution factors are based on the severity of reflective cracking in the asphalt and the condition of the tie rods. The as-is condition of the ARB had areas of moderate and severe reflective cracking, which corresponds to a recommended load distribution factor of 0.5.

Table 6.2 Distribution factor recommendations (WSP report).

Reflective Crack Condition	Tie Rod Condition	Recommended DF (Lane)
None/Minor	Good	Follow AASHTO
Moderate	Good	0.35
Severe	Good	0.5
Any Condition	Poor/Loose	0.5

The American Association of State Highway and Transportation Officials (AASHTO) provides equations for calculating the distribution factors of live loads per lane for interior beams. For the ARB, the AASHTO calculated distribution factor was 0.262 for the interior girders.

Table 6.3 summarizes the distribution factors that were calculated from the measured displacements. The values in the table represent the worst case for a given test and truck position. For context, a distribution factor of 0.10 would mean that the weight of the truck was equally distributed to all ten channel girders, whereas a distribution factor of 0.5 signifies that each girder is experiencing one wheel line of load, and substantially less load is being transferred between adjacent channels.

Table 6.3 Summary of experimentally determined distribution factors.

	12-Sep	7-Nov	28-Nov	8-May	8-May
Truck Position	As-Is	No tie rods, no PT	PT only	PT & LMC	LMC only
1	0.250	0.259	0.241	0.224	0.221
2	0.240	0.223	0.181	0.172	0.171
3	0.203	0.188	0.160	0.172	0.175
4	0.239	0.235	0.170	0.176	0.176
5	0.260	0.249	0.226	0.227	0.222

The highest measured distribution factor (worst load distribution) was 0.260, from the loading of truck position 5 in the as-is condition. Exterior truck positions consistently showed higher distribution factors because the exterior girders cannot effectively distribute load in the transverse direction. This leads to the highest DFs being recorded on the first or second interior girders. When considering only the interior truck positions (positions 2, 3, and 4), the highest distribution factor was 0.240 at positions 2 and 4 during testing for the as-is condition.

There is little change in distribution factors between the as is condition and the removal of tie rods. In fact, in four positions the distribution factors were improved after the tie-rods had been removed. This is not attributed to an actual improvement due to removal of tie rods. Rather is attributed to variability in the measurement potentially combined with environmental effects. The variability ranged from 4.11 to 7.55 percent. The data suggests that the tie rods did not significantly contribute to the overall distribution of loads on the bridge.

The addition of PT resulted in distribution factors of 0.18, 0.16 and 0.17 for truck positions two, three, and four, respectively. Compared to the as-is condition, this corresponds to improvements of 25%, 21%, and 29%, respectively in terms of lateral load distribution. During this series of tests, position 3 yielded the lowest distribution factor of all tests at 0.16.

The PT plus LMC condition resulted in distribution factors that were up to 28% lower than the as-is condition. Three of the five truck positions have distribution factors equal to, or higher than, those in their respective PT-only condition. This may be partially due to the loss of prestress force between the test dates.

Testing after removing PT resulted in distribution factors similar to those calculated for the PT plus LMC condition. The similarity may be due to locked-in compression between the channels.

Table 6.4 summarizes the percentage difference in distribution factors between the as-is condition and other tests performed on the bridge. Comparing distribution factors in this manner enables a straightforward comparison. All positive values correspond to improved load distribution (resulting in decreased distribution factors).

Considering interior truck positions only, the addition of PT greatly improved the distribution factors as they decreased by between 21% and nearly 29%. Except for truck position 3, similar results were observed in the LMC plus PT and LMC-only conditions. While the presence of LMC had mixed results relative to the PT-only condition, overlays may potentially lead to more durable and longer lasting bridges.

Having been recently placed and lightly used, the LMC overlay was in excellent condition during testing. As such, the results of the final test are a best-case scenario for the LMC-only condition. If a similarly detailed and installed LMC overlay were applied to an in-service bridge without also installing XPT, it is likely that the LMC would soon develop reflective cracks at the channel-channel joints. The reflective cracks would diminish the durability and load distribution effects of the LMC. Hence, it is recommended that XPT be installed along with any LMC that is similar to the overlay placed on the ARB test bridge.

Table 6.4 Percent difference in DF compared to the as-is condition.

	12-Sep	**7-Nov**	**28-Nov**	**8-May***	**8-May****
Truck Position	As-Is	No tie rods, no PT	PT only	PT & LMC	LMC only
1	-	-3.47	3.54	10.6	11.5
2	-	6.89	24.7	28.3	28.5
3	-	7.55	21.0	15.4	14.0
4	-	1.53	28.8	26.4	26.5
5	-	4.11	12.8	12.7	14.5

6.5 Potential Improvement in South Carolina Load Ratings

A load rating on a bridge is an indication of how safely the bridge can carry legally permissible loads. This rating evaluates multiple components of a bridge, including structural capacity, material strength, and existing conditions. A load rating greater than 1.0 means that a bridge has the structural capacity to carry legal loads safely. In contrast, a load rating factor less than 1.0 means that a bridge is unsatisfactory and may be posted to restrict the weight limit on the bridge.

Eubanks (2023) obtained load rating data for 95 skinny-leg channel bridges in upstate South Carolina. The load ratings are based on an EV3 vehicle, a tri-axle truck with a 24-kip front axle and two 31-kip rear axles. Figure 6.5 is adapted from Eubanks (2026) and shows the distribution of skinny leg channel girder bridges based on the EV3 vehicle. A marker at a load rating of 1.0 distinguishes unsatisfactory bridges – falling below the required strength for legal loads – and those capable of supporting such loads. Of the 95 bridges on the graph, 92 are below strength.

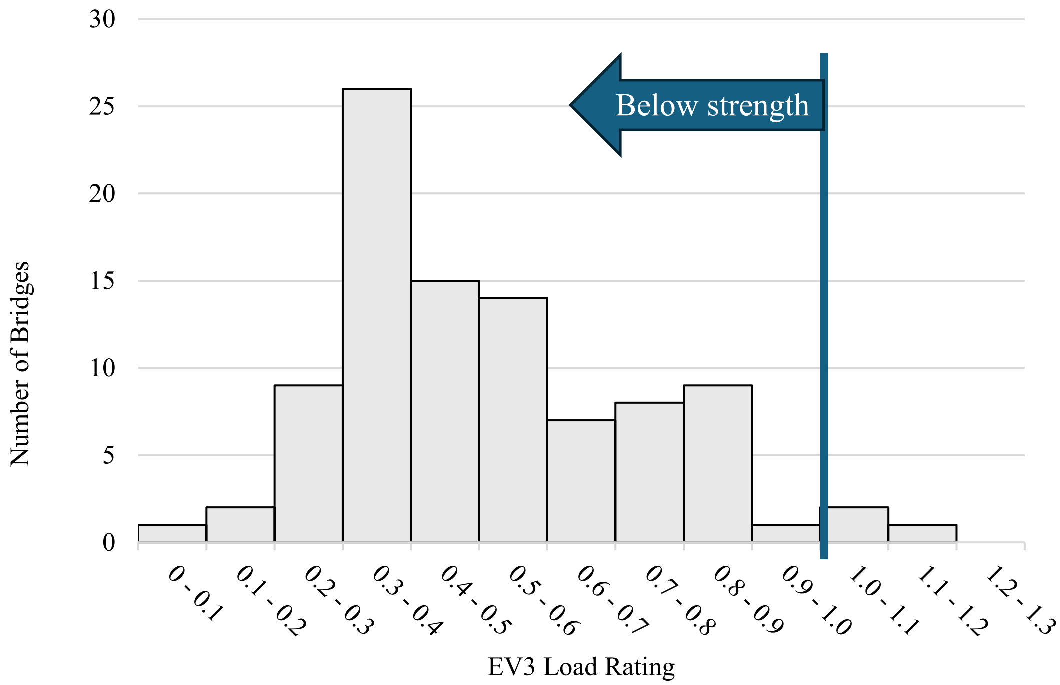

Figure 6.5 Distribution of prestressed skinny leg channel girder bridge load ratings.

The load rating data consider final values. The potential effects of retrofitting may be estimated, however, by assuming inventory-wide improvement in load distribution. Further, it may be reasonable to assume that the percentage of improvement in load distribution will correspond to the same level of reduction in load rating. For example, a 30% improvement in load distribution may be assumed to correspond to a 30% increase in load rating.

Referring to Table 6.4, the application of transverse post-tensioning improved load distribution in the interior lanes by at least 21% relative to the as is condition. Assuming a 20% improvement is achieved by retrofitting the SC inventory of skinny-leg channel bridges, the load ratings shown in Figure 6.6 are produced. In this hypothetical scenario, the retrofits would lead to 10 additional bridges with satisfactory load ratings.

It is possible that retrofits may affect load ratings by more than 20%. The highest (worst) experimental distribution factor from the retrofit conditions and interior truck paths was 0.181 (Table 6.3). The lowest (best) distribution factor recommended in the WSP report (Table 6.2) is the AASHTO-calculated value. According to Waters (2024), the AASHTO-calculated value for the ARB is 0.262. Comparing these values, the worst measured distribution factor is approximately 30% better than the best of the recommended values (0.181 compared to 0.262). Increasing the load rating for all bridges (Figure 6.5) by 30% would result in 22 bridges with satisfactory ratings (i.e., >1.0).

Given the condition of the tie rods and the presence of reflective cracking in the pavement on skinny-leg channel girder bridges, it is likely that the load rating data in Figure 6.5 were based on distribution factors of 0.35 and 0.50 (Table 6.2). In comparison, the experimental distribution factor of 0.181 (Table 6.3) is 48% to 64% better. Assuming that retrofits were applied and resulted in a 50% improvement in distribution factors and load ratings, the data shown in Figure 6.7 is obtained. In this hypothetical scenario, 42 of the 95 (44%) skinny leg channel bridges would obtain satisfactory load ratings.

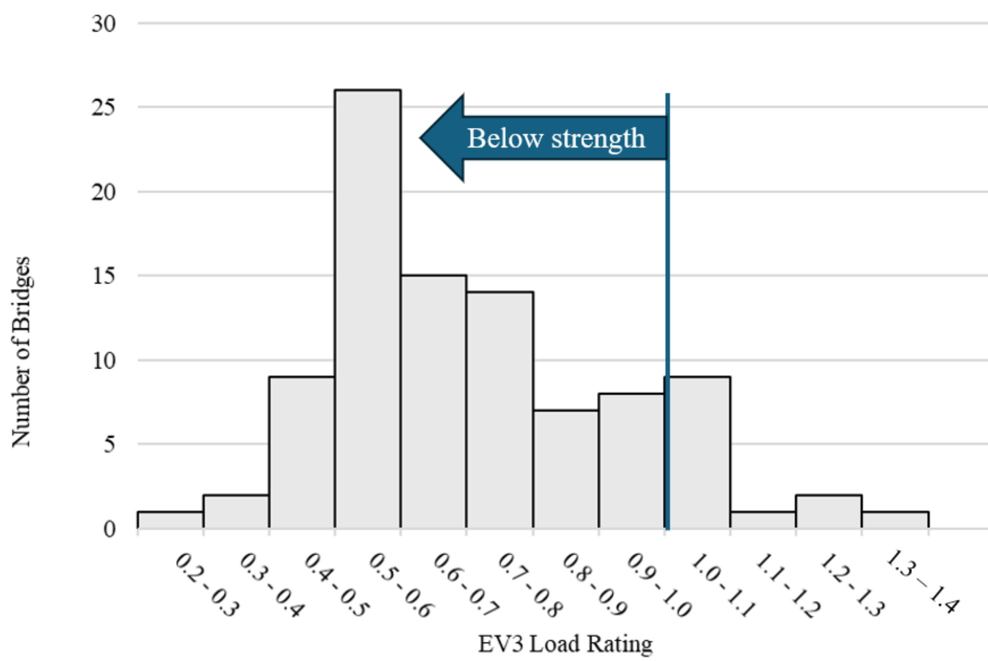

Figure 6.6 Prestressed skinny leg channel girder bridge load ratings, assuming retrofits provide a 20% improvement in load distribution.

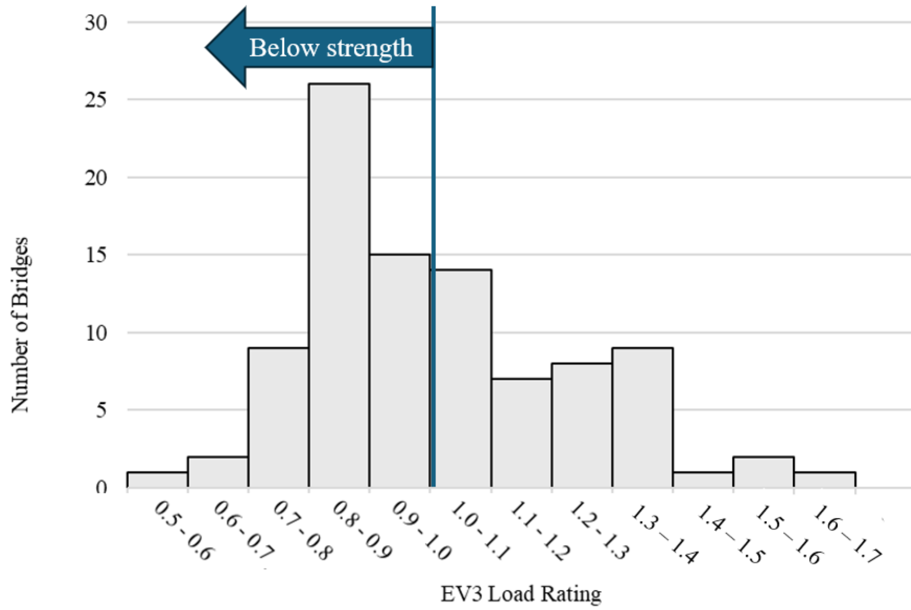

Figure 6.7 Prestressed skinny leg channel girder bridge load ratings, assuming retrofits provide a 50% improvement in load distribution.

These estimates, though simplified, demonstrate the potential of XPT and XPT+LMC retrofits. The improvements in load distribution from these retrofits may potentially lead to removal of load postings for approximately 40 additional skinny leg channel girder bridges. While not addressed here, it seems likely that similar retrofits would also have beneficial applications for wide leg channel bridges.

6.6 Conclusions

Transverse post-tensioning alone provided an improvement in lateral load distribution of over 20% (relative to the as-is condition) for interior channel girders. The latex-modified concrete overlay, alone or in combination with transverse post-tensioning, provided similar benefits in terms of load distribution. As expected, both retrofits had a greater impact on interior channel girders than on exterior girders. Though simplified approaches were used, the improvements in load distribution from the retrofit have potential to justify removal of load postings from a substantial number of skinny leg channel bridges and warrant further consideration.

CHAPTER 7: STATIC LOADING OF CHANNEL GIRDERS WITH LMC OVERLAY

7.1 Summary and Key Takeaways

- LMC topped channel girders were tested to evaluate the impact (if any) of the LMC on capacity and failure behavior.
- The experimental capacities of the LMC topped specimens exceeded the calculated nominal capacity by 17% to 27%.
- In three of the four test specimens, the LMC delaminated from the channel girder before reaching flexural failure.
- LMC contributions to strength should be neglected unless the interface surface is more aggressively prepared.

7.2 Introduction and Specimen Details

Four skinny leg channel girders with LMC topping were tested in flexure under quasi-static loading. The primary intents of testing were to evaluate the impact (if any) of the LMC topping on flexural capacity and to determine if the LMC remained composite with the channel up to flexural failure. The channel girders and LMC for flexural testing were previously used in service-level testing (Table 7.1).

Table 7.1 Flexural test specimens with LMC topping.

Specimen ID	LMC and test details	LMC placement date	Load test date	Source of channel girder	Surface preparation for LMC
L1	Chapter 5	July 2023	November 2023	SCDOT Saluda yard	3,000 psi (max) pressure wash
L2	Chapter 5	July 2023	February 2024	SCDOT Saluda yard	3,000 psi (max) pressure wash
L3	Chapter 6	April 2024	October 2024	Airport Road, Greenwood	Abraded during topping removal, then 3,200 psi (max.) pressure wash
L4	Chapter 6	April 2024	July 2025	Airport Road, Greenwood	Abraded during topping removal, then 3,200 psi (max.) pressure wash

7.3 Calculated capacity and cracking moment

Nominal flexural capacities were calculated using the methodology outlined in AASHTO LRFD, 2017, Section 5.6.3.1 and the properties listed in Table 7.2. Calculations for the LMC-topped channels assume composite action between the LMC and channel girder. The calculated capacities were based on the cross-section at midspan. Due to the harped strands and 4-point loading scheme, the critical section for moment capacity is below the load points rather than at midspan. While the nominal capacity at the critical section is approximately 6% smaller than at mid-span, the mid-span capacity provides a convenient value for comparison. In addition to listing the calculation inputs, Table 7.2 also includes the calculated capacities. The presence of a composite LMC topping increases the moment of inertia by 42% and the nominal flexural capacity by 17% relative to the baseline.

Table 7.2 Inputs and results of capacity calculations.

Property	LMC-topped channel girder	Baseline channel girder
*Concrete compressive strength	5,000 psi	5,000 psi
*Concrete tensile strength	530 psi	530 psi
Section moment of inertia	6,835 in^4	4,823 in^4
Section centroid from the bottom of the precast	13.12 in.	11.83 in.
Strand ultimate strength	250 ksi	250 ksi
Effective prestress	140 ksi	140 ksi
Effective strand depth at mid-span	14.63 in	12.63 in
Area of prestressing	0.8 in^2	0.8 in^2
Width of compression face	33 in	33 in
Calculated self-weight moment at mid-span	35.4 kip-ft	28.0 kip-ft
Calculated cracking moment (after self-weight has already been applied)	86.1 kip-ft	74.8 kip-ft
Calculated cracking moment	122 kip-ft	103 kip-ft
Calculated nominal moment capacity at mid-span	222 kip-ft	189 kip-ft
* The same concrete properties were assumed for the LMC and precast. This simplification has a negligible effect on the calculations.		

Given the possibility of horizontal shear failure at the LMC-precast interface, the nominal interface shear capacity is also of interest. AASHTO LRFD, 2017, Section 5.8.4 combines the effects of cohesion and shear-friction when determining interface capacity. No reinforcement crossed the interface in the test specimens; thus, shear-friction did not contribute to the interface capacity. Thus, according to AASHTO, the nominal strength of the interface is 0.075 ksi, which is the cohesion contribution and is based on concrete cast against a “clean concrete surface, free of laitance, but not intentionally roughened.”

7.4 Results and Discussion

The midspan moment-displacement responses of the LMC-topped specimens are shown in Figure 7.1. The moment includes the effect of applied loads and self-weight. To provide context for the experimental results, the figure also displays calculated capacities. Additionally, the response from USC Test #2 is included for comparison. This specimen was selected for comparison because it originated from the same source as specimens L1 and L2, and because its moment-displacement response is in the middle range of similar baseline specimens. The response of specimen L4 is not shown in Figure 7.1 because the data was lost due to sudden loss of power.

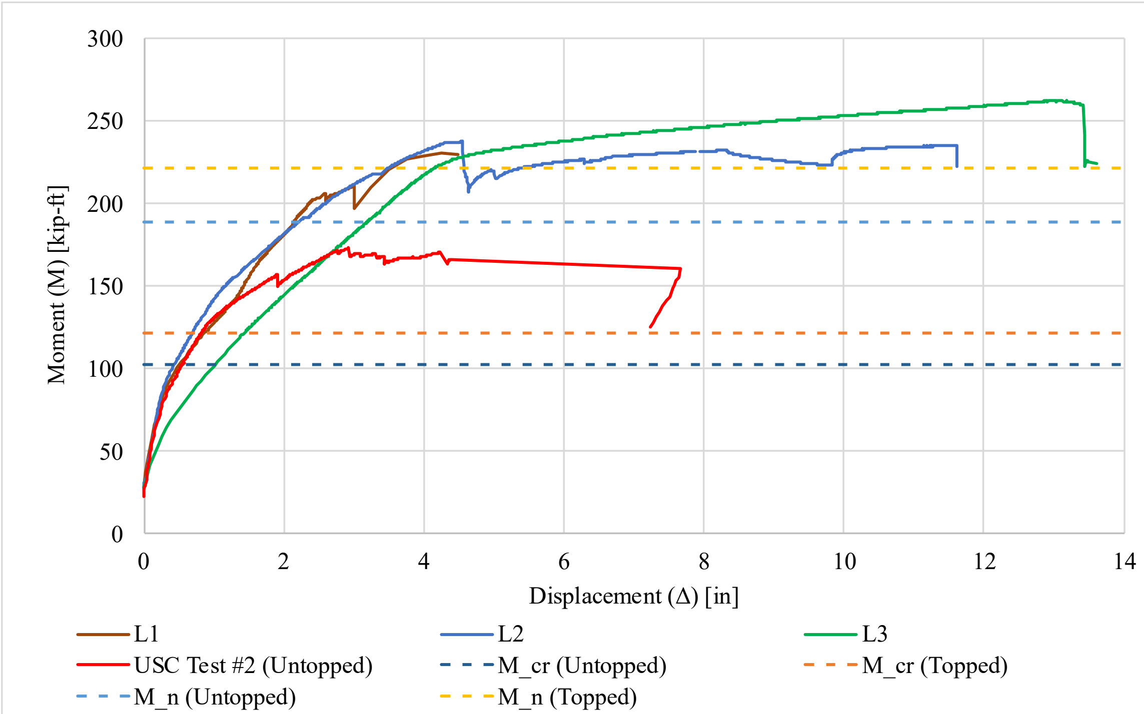

Figure 0.1 Moment-displacement response of test specimens with LMC topping (response of a baseline channel girder and calculated capacities are shown for context).

Specimens L1 and L2 were sourced from the same location, had similar surface preparation, and had LMC placed at the same time using the same mix. Both specimens responded linear-elastically at moments less than 80 kip-ft., after which flexural cracks opened. The calculated cracking moment for the LMC-topped section of 122 kip-ft. was larger than the experimentally observed cracking moment. This result is attributed to preexisting cracks that likely formed while the channel girders were in service on a bridge before being salvaged and stored at the SCDOT Saluda yard. Although the provenance of channels L1 and L2 is unknown bridge components are commonly stored by SCDOT after they are removed from bridges. The calculated cracking moments include the tensile strength of the concrete, which was likely absent in L1 and L2 due to pre-existing flexural cracks.

The failure of L1 occurred in two stages. At 210 kip-ft. the LMC topping delaminated from the girder (Figure 7.2), resulting in an abrupt drop in load. After delamination, the applied moment was resisted by the non-composite precast section alone. Testing continued up to a peak moment of 228 kip-ft., which corresponded with strands rupturing at a section below one of the load points. Rupturing of the strands was accompanied by a large crack and crushing of the concrete compression flange (Figure 7.3).

The failure of specimen L2 also involved LMC delamination and strand rupture. A portion of the LMC-topping delaminated from L2 at a moment of 240 kip-ft. The delamination was accompanied by an abrupt drop in load. Testing continued after the delamination; however, the moment never exceeded the previous peak. Specimen L2 withstood over 11 in. of displacement before strands ruptured at the section below one of the load points (Figure 7.4).

Figure 0.2 Delamination of LMC on girder L1.

Figure 0.3 Failure of girder L1 due to strand rupture below load point.

Figure 0.4 Failure of specimen L2 (left); and L3 (right).

The initial stiffness of L3 was less than that of L1, L2, and the baseline (USC Test #2). While the reason(s) are not known, a likely cause is the extent and severity of pre-existing flexural cracks.

Although its initial stiffness was lower, its post-cracking and final stiffness were comparable to those of the other channels.

L3 reached a peak moment of 260 kip-ft., which corresponded to a displacement of approximately 13 in. At the peak moment, the LMC topping crushed in compression near one of the load points. The LMC topping remained bonded to and fully composite with the precast channel girder throughout the test. Because the LMC topping remained bonded, L3 supported a higher experimental moment than L1 and L2, which experienced delamination of the topping.

Likely reasons for specimen L3's distinct bond performance include surface preparation and LMC mix design. Recall that L3 was sourced from the bridge described in Chapter 6. The pavement on top of the bridge was removed by scraping the surface using a bucket with metal tines. In addition to removing the pavement, the bucket tines also abraded the precast surface, loosening any weak material. In contrast, pavement was likely removed from L1 and L2 many years prior to their use in the test program. The pavement removal could have been less abrasive, and the concrete surface material may have weakened while channel L1 and L2 were sitting in outdoor storage. Before placing LMC, the top surfaces of the precast channels were cleaned with a high-pressure water spray. The pressure washer used to clean the surface of L3 had a reported maximum pressure of 3,200 psi, which is slightly larger than the 3,000 psi maximum pressure for the machine used to clean L1 and L2. The mix design for the LMC topping was different between L3 and the mix from L1 and L2. L1 and L2 used a rapid-set LMC mix, which began to harden toward the end of placement, making it difficult to place and finish.

Specimen L4 originated from the same bridge, underwent the same surface preparation, and used the same LMC mix as Specimen L3. Unfortunately, data from the L4 test was lost due to sudden loss of power during testing. However, test notes, photos, and videos indicate that the topping slab delaminated from one half of the span at approximately the same time as the peak load was reached. The specimen continued to displace until the top of the precast crushed in compression (Figure 7.5).

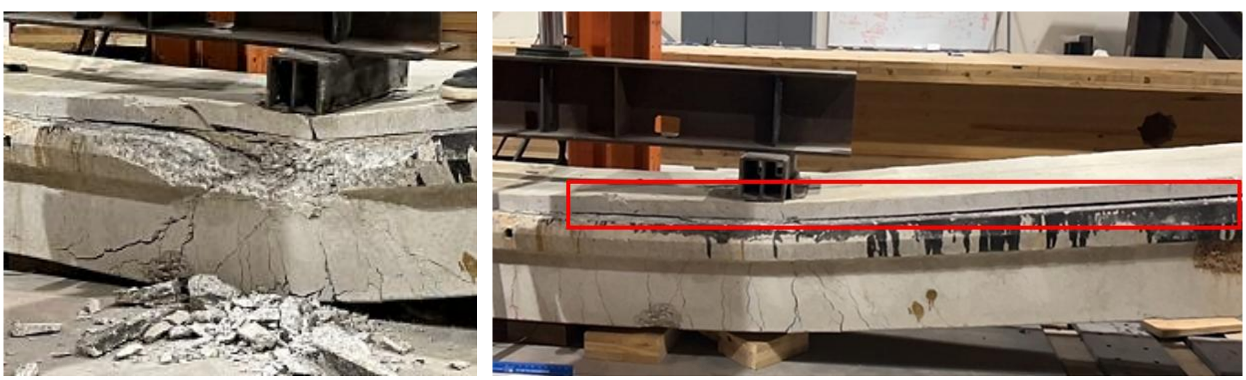

Figure 7.5 Flexural failure of L4 (left); and topping delamination before failure (right).

7.5 Comparison of Experimental and Calculated Nominal Capacities

Elastic beam theory was used to calculate the interface shear stress for specimens L1, L2, and L3 (Equation 7.1). This approach is an oversimplification because flexural cracking in the specimens caused variable section properties along the span, resulting in higher interface stresses at sections with cracks. Hence, results from this approach are a lower bound of the interface stresses in the specimens. The approach remains useful for comparisons between specimens and against the

AASHTO LRFD nominal interface capacity of 0.075 ksi (Table 7.3). The lower-bound experimental shear stresses were approximately half of the AASHTO LRFD nominal capacity. It is likely that the interface stress at the sections with flexural cracks was closer to the AASHTO LRFD value.

$$\tau = \frac{VQ}{Ib} \qquad \text{Equation 7.1}$$

Where:

τ =	Interface shear stress
V =	Shear force (taken as the experimental shear at delamination or flexural failure)
Q =	First moment about the composite section centroid of the LMC topping
I =	Composite section moment of inertia
B =	Width of interface

Table 7.3 Comparison of experimental and nominal interface shear stress.

Specimen	Experimental shear stress at interface (lower bound)	AASHTO LRFD nominal interface shear capacity	Experiment to nominal ratio	Notes
L1	0.037 ksi	0.075 ksi	0.49	Based on the shear force coinciding with topping delamination
L2	0.042 ksi		0.56	Based on the shear force coinciding with topping delamination
L3	0.045 ksi		0.60	Based shear force at flexural failure

Experimental and calculated flexural capacities are compared in Table 7.4. Experimental capacities exceeded the nominal flexural capacity of the LMC-topped cross-sections. The differences between experimental and theoretical capacities are even greater than those shown in the table because the critical section for flexure was at the load points. At this location, the experimental moment was approximately the same as shown in Table 7.4; however, the nominal capacity was lower due to reduced internal moment arm from the harped strands. Furthermore, the LMC topping on specimens L1 and L2 delaminated before flexural failure; thus, a comparison with the nominal capacity of the baseline specimen is approximate. The experimental capacities of L1 and L2 were 21% and 27% higher, respectively, than the nominal capacity of the baseline cross-section.

The increased experimental flexural capacity relative to nominal is attributed to multiple factors. The calculations assumed a 250 ksi ultimate strength for the strands; however, as demonstrated from the strand tests discussed in Chapter 3, the strand capacity was likely higher than the assumed value. While bearing pads were used at the supports, horizontal reactions were present to some degree and likely contributed to arching action and increased specimen capacity. Finally, the concrete compressive strengths may have been higher than the assumed values. The difference in concrete strengths would have a smaller impact on specimen capacity than the stand properties and arching action.

Despite the higher than theoretical experimental capacities, it is recommended that the effects of LMC topping be neglected in theoretical capacity calculations. The LMC topping delaminated from three of four specimens prior to flexural failure. It is possible that more aggressive surface preparation and alternative LMC mixes would support full composite action; however, composite action should not be relied upon when calculating the nominal flexural capacity of a channel girder having similar surface preparation to the experiments.

Table 7.4 Comparison of experimental and nominal flexure capacities. Italicized and underlined values indicate ratios with consistency between the theoretical cross-section and the experimental failure mode.

Specimen	Max experimental moment	Calculated nominal moment (w/ LMC topping)	Experiment to nominal ratio (LMC topping)	Calculated nominal moment (untopped)	Experiment to nominal ratio (untopped)
L1	228 kip-ft.	222 kip-ft.	1.03	189 kip-ft.	*1.21*
L2	240 kip-ft.		1.08		*1.27*
L3	260 kip-ft.		*1.17*		1.38

7.6 Conclusions and Recommendations

Four LMC-topped channel girder specimens were loaded to flexural failure. Before installing the LMC overlays the surfaces of the precast channels were cleaned with pressure washers having a maximum pressure of up to 3,200 psi. Based on experimental and calculated results the following conclusions and recommendations are made:

- Surface preparation was insufficient to ensure composite action at failure loads. The LMC topping on three of the four specimens delaminated before reaching flexural failure.
- Experimental capacities exceeded the corresponding calculated nominal capacities by 17% to 27%. Increased capacity is attributed to higher-than-assumed strand properties and boundary conditions that generate arching action.
- For the tested level of surface preparation and materials it is recommended that the LMC topping be neglected when calculating the nominal flexural capacity.
- Aggressive substrate preparation, such as hydro-demolition or high-pressure cleaning, is likely to improve composite action between the precast channels and LMC topping. The LMC supplier recommends a 7,000 psi pressure washing value, which is more than double the pressure used to prepare the test specimens.

CHAPTER 8: CYCLIC LOADING OF CHANNEL GIRDERS WITH LMC OVERLAY

8.1 Summary and Key Takeaways

- Two LMC-topped channel girders were tested under hundreds of thousands of service load cycles.
- The LMC topping remained bonded to the channel girder specimens throughout the load cycles.
- One of the specimens failed due to strand rupture; a failure mode that can also affect untopped channel girders. The embedded strand hold-down device at midspan likely caused stress concentrations in the strands, leading to their failure.
- Flexural cracks near midspan of skinny-leg channel girders may be an early warning of vulnerability to failure at less than nominal capacity. Inspectors should give special attention to cracks that remain open even when truck loads are not present.

8.2 Introduction

Cyclic load tests were conducted to evaluate the performance of channel girders topped with latex-modified concrete (LMC) under simulated, repeated traffic loads. Two specimens, CL1 and CL2, were tested, both coming from the Airport Road Bridge discussed in Chapter 6.

National Bridge Inventory (NBI 2024) data were used to determine the target number of load cycles. Table 8.1 summarizes the average daily truck counts for skinny-leg channel bridges in SC. According to the data, approximately 90% of these bridges are expected to support around 530,000 truck crossings in a ten-year period. Accordingly, the target for testing was set to 600,000 load cycles.

Table 8.1 Skinny-leg channel average truck traffic.

Measure	Count
90th Percentile (10-year)	529,250
90th Percentile (daily)	145
80th Percentile (daily)	75
Maximum (daily)	792
Median (daily)	16
Average (daily)	55

8.3 Methodology

Unless noted otherwise, the same methodology was used for both CL1 and CL2. Upon arrival at the lab, the condition of the LMC topping was assessed and documented. Chain dragging was used to “sound” the LMC and identify any areas of delamination. Load cycles began soon after evaluating the LMC-precast interface for delamination. Consistent with the tests reported in previous chapters, the cyclic load testing utilized a four-point bending setup (Figures 8.1 and 8.2). Bearing pads were placed at the bearing points below each stem at both ends of the channel.

Loads were applied to generate the conditions described in Table 8.2. “Equivalent” lab loads were calculated such that the experimental moment in the test specimen corresponded to a specific design truck, distribution factor, and impact factor. This approach was necessary because the axle spacings on the design trucks differ from the load point spacing in the lab setup. Design trucks and impact factors were based on AASHTO LRFD (AASHTO 2017). Distribution factors were selected after considering the results from Chapter 6. Condition "A" is distinct in that it is based on the range of the elastic response rather than a truck load and design moment. The load for the elastic condition was determined from previous tests of skinny-leg channel girders; results of the elastic stage provided basic information about the specimen's condition before simulated truck loadings were applied. Stages with H15 loading were intended to approximate service-level conditions, and the stage with HL-93 loading approximated overload conditions.

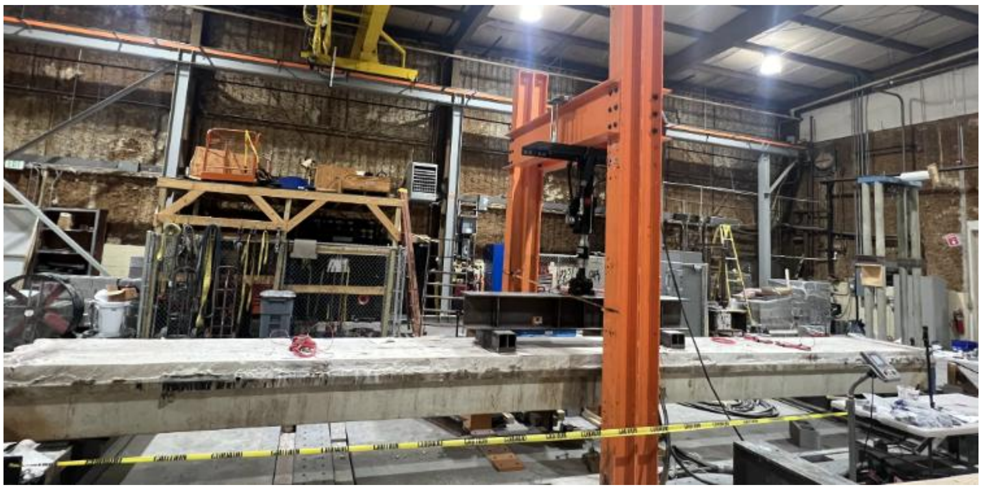

Figure 8.1 Photograph of cycle load test setup.

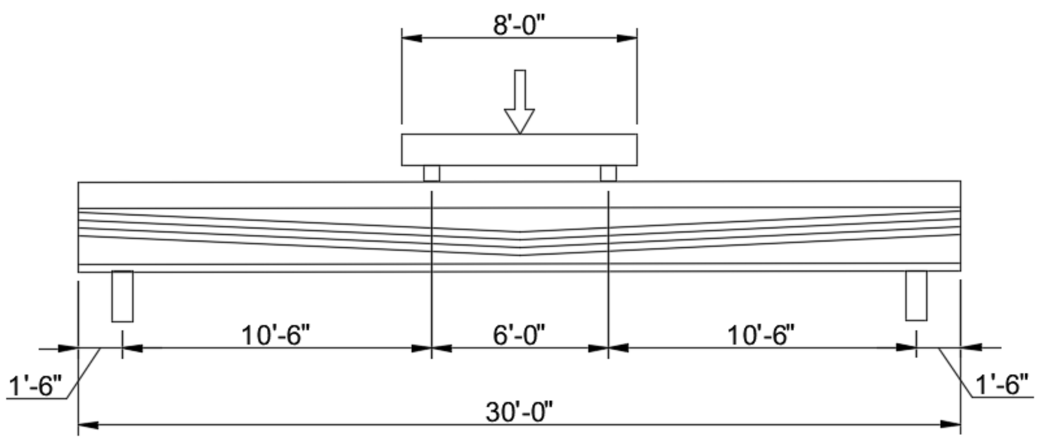

Figure 8.2 Geometry of cycle load test setup.

Table 8.2 Loading conditions and equivalent actuator loads.

Condition label	Truck	Axle Load (kip)	DF	IM	Load/axle (kip)	Design moment (kip-ft)	Equivalent actuator load** (kip)
A (elastic)	NA	NA	NA	NA	NA	47	9.0
B	H15	24	0.25	1.33	8.0	60	11.5
C	H15	23	0.30	1.33	9.6	72	14
D	H15	24	0.35	1.33	11.2	84	16
E	HL-93*	32	0.30	1.33	13	96	18.5
* Lane load not included ** Force applied by the actuator such that the experimental moment equaled the design moment							

The overall approach was to test and evaluate the specimens in stages, beginning with the elastic condition (A) and then moving through the cycles with higher loads. The conditions, load ranges, and number of cycles are reported in Table 8.3 for CL1 and Table 8.4 for CL2. The minimum load was maintained at three kips for each stage and simulated the effect of pavement dead load. For stages representing truck loads the upper load includes the equivalent actuator load plus three kips for pavement dead load. The loading frequency was between 0.8 Hz to 1.3 Hz, with faster cycles being applied to lower load levels.

CL1 was tested first and failed before reaching the target number of cycles. Based on the results of CL1, the load levels for CL2 were reduced by reconsidering the distribution factor used for calculating the design moment and equivalent actuator load (Table 8.2). The distribution factor was reduced from 0.35 to 0.30 or 0.25. The improved (lower) distribution factors are within the range of values observed in the as-is (prior to retrofit) tests of the Airport Road Bridge reported in Chapter 6.

Table 8.3 Loading stages for CL1.

Stage	Condition	Load Range (kip)	Number of Cycles	Cumulative Cycles
1	A (elastic)	3 – 9	200,0000	0 – 200,000
2	D (H15, DF=0.35)	3 – 19	419,028	200,001 – 619,028*
* Stage ended with specimen failure				

Table 8.4 Loading stages for CL2.

Stage	Condition	Load Range (kip)	Cycles	Cumulative Cycles
1	A (elastic)	3 – 9	200,000	0 – 200,000
2	B (H15)	3 – 15	600,000	200,001 – 800,000
3	C (H15)	3 – 17	450,000	800,001 – 1,250,000
4	E (HL-93)	3 – 21	50,000	1,250,001 – 1,300,000

Specimen stiffness and LMC-channel bond were evaluated during “measurement cycles” conducted at intervals corresponding to each order of magnitude of load cycles (10, 100, 1000...). Each set of measurement cycles included collecting load and displacement for 10 cycles. These data were used to determine the elastic stiffness of the specimen, which is defined as the average stiffness across the 10 cycles for loads between three and nine kips. For stages that exceeded nine kips, the inelastic stiffness was also determined for the load range between nine kips and the maximum applied load. After the measurement cycles, the LMC topping was chain-dragged to check for delamination, and visual inspection was conducted to confirm that there was no movement of the girder on the supports and that the actuator remained correctly aligned.

8.4 Results – CL1

During the evaluation prior to loading, delaminated areas of the LMC topping were identified at both ends of specimen CL1. The delamination occurred sometime during removal from the Airport Road Bridge or delivery of the lab in Clemson. The delamination was limited to the ends of CL1 in the portion of the specimen that extended beyond the supports (Figure 8.3).

Figure 8.3 CL1 LMC delamination (highlighted in red) at north end (left); and south end (right).

As expected, specimen CL1 had greater stiffness compared to an untopped baseline channel girder. Within the elastic range, the LMC-topped girder had approximately 40% more stiffness (Figure 8.4). Specimen CL1 maintained stiffness without any signs of topping delamination or girder cracking during the elastic stage.

Flexural cracks (Figure 8.5) were observed in both stems of specimen CL1 after the first cycle of the H15 stage (n = 200,001). Flexural cracking corresponded to a 10% reduction in elastic stiffness (52.6 kip/in. to 47.2 kip/in) (Figure 8.6).

Damage to CL1 accumulated over the course of the H15 load stage. Between cycles 200,000 and 201,000, the inelastic stiffness of the girder decreased by 4% (22.8 kip/in. to 21.8 kip/in) (Figure 8.7). The inelastic stiffness continued to reduce at cycles above 201,000, but at a reduced rate. At 384,380 cycles into the H15 load stage (584,380 cumulative cycles), an audible popping sound indicated that a wire or strand had snapped; upon unloading, a residual flexural crack having a width of approximately 0.035 inches was observed in one of the stems. Small areas of LMC delamination were also identified in the high-shear zones between the load points and supports. The delamination was identified using chain dragging and covered an area of approximately three to four square feet. The snapped wire and partial LMC delamination resulted in abrupt changes in elastic (Figure 8.5) and inelastic stiffness (Figure 8.6).

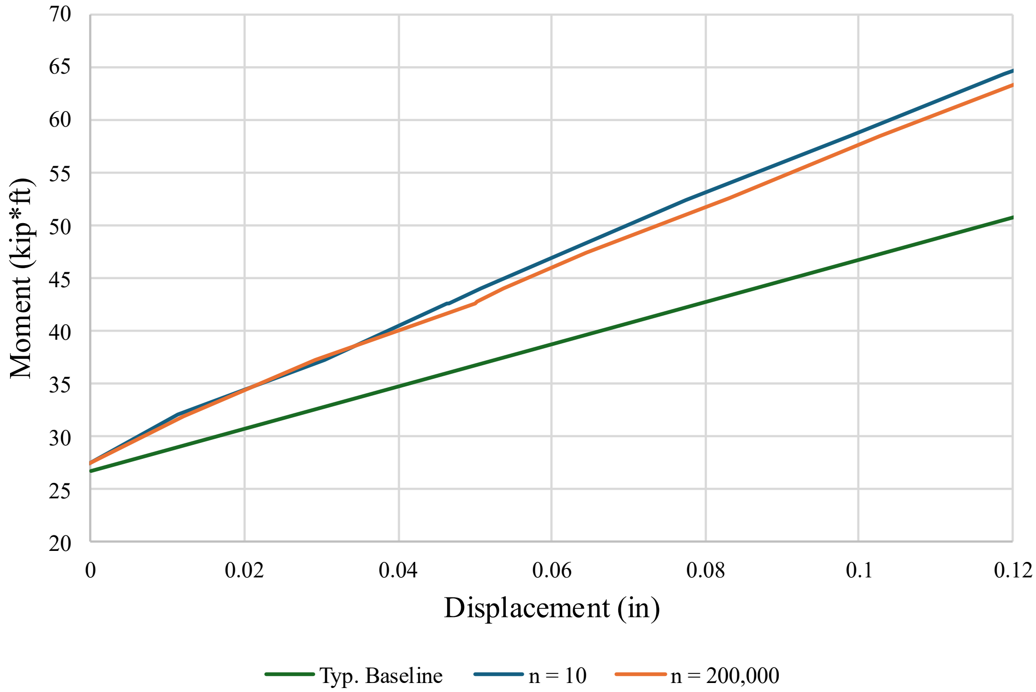

Figure 8.4 Elastic moment vs. displacement of CL1 and baseline.

Figure 8.5 CL1: Flexural cracking at midspan after initial service level cycles.

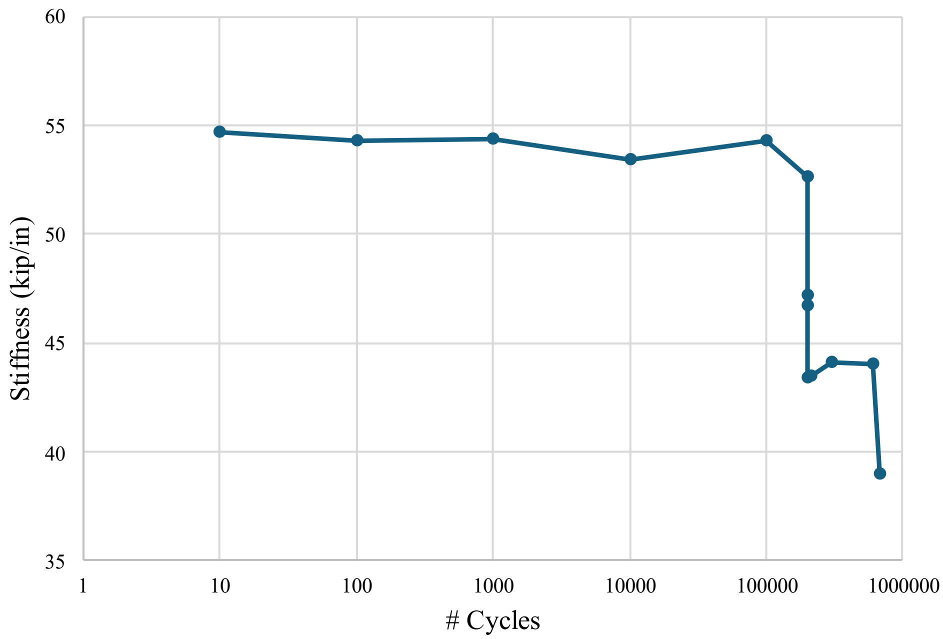

Figure 8.6 CL1: Elastic stiffness (3 to 9 kips) vs. completed cycles

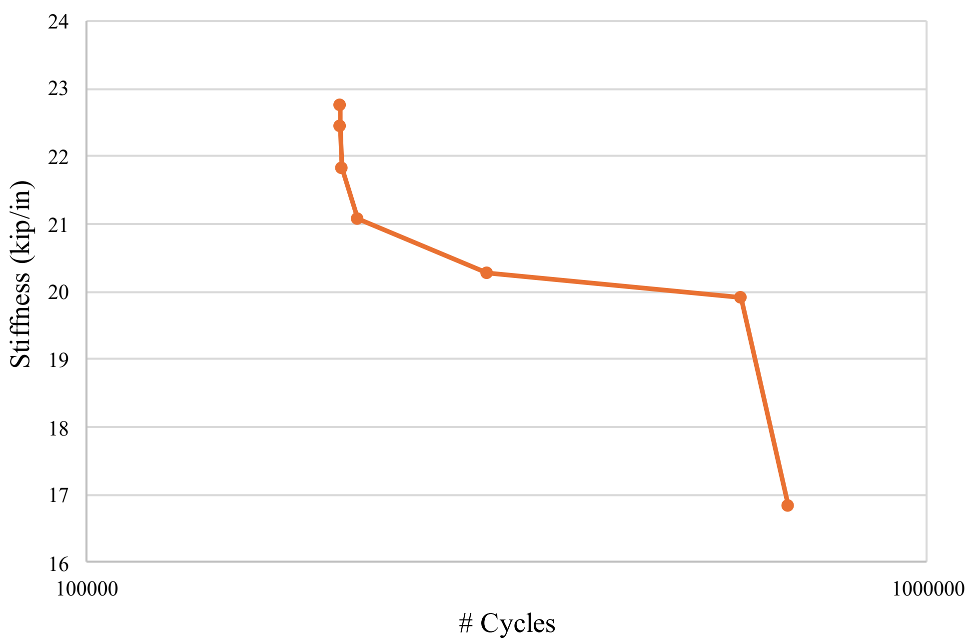

Figure 8.7 CL1: Inelastic stiffness (9 to 19 kips) vs. completed cycles.

Loading was resumed after the events at cycle 384,380. At 419,028 cycles into the H15 load stage (619,028 cumulative cycles), multiple strands ruptured in one of the stems, leading to flexural failure (Figure 8.8) and delamination of the LMC topping. The LMC delamination occurred throughout the area between the loading points. The failure was abrupt and resulted in a sudden loss of load. The timeline of events leading to failure is summarized in Table 8.5.

Figure 8.8 Flexural cracking and LMC delamination after 619,028 cycles.

Table 8.5 Specimen CL1 events and observations.

Load Range (kip)	Cumulative # Cycles	Event / Observation
Elastic (3 - 9)	0 - 200,000	Elastic response, stiffness maintained
H15, Service (3 - 19)	200,001	Flexural cracks at midspan and loss of stiffness. Cracks closed upon unloading.
	200,001 - 201,000	Cumulative damage resulting in stiffness loss
	201,001 - 384,379	Stiffness loss at a reduced rate
	584,380	Audible sound suggesting a wire or strand snap. Crack width ~0.035 in. after load removed. Minor delamination in the topping.
	584,381 - 619,027	No significant events or observations.
	619,028	Strand rupture and flexural failure with accompanying LMC delamination.

After failure, it was determined that the strands ruptured near the embedded hold-down device (also called a harping point) at midspan (Figure 8.9). The edges of the hold-down device were sharp and likely produced stress concentrations in the strands, which would have repeated through thousands of load cycles, eventually leading to strand rupture. It is likely that strand rupture originated with the lowest harped strand. During the post-failure investigation, it was determined that all strands in the problematic stem ruptured, the LMC topping delaminated, and significant flexural cracking occurred in the opposite stem. Strand rupture is considered the primary failure, with LMC delamination and other flexural cracking as secondary events.

Figure 8.9 Hold-down device and ruptured strands (left) and hold-down device (right).

8.5 Results – CL2

Prior to loading delamination of the LMC topping was observed at the ends of specimen CL2 at locations similar to specimen CL1 (Figure 8.3). Delamination was not observed in the area between the supports. Portions of the LMC topping that were bonded before loading remained bonded throughout the 1,300,000 load cycles of the test program.

The elastic stiffness of CL2 partially diminished after the load was increased from the elastic stage to the first H15 truck loading stage (Figure 8.10). The loss of stiffness corresponded to the opening of flexural cracks. The elastic and inelastic stiffness dropped when the maximum load was increased at cycle 800,001 and again at cycle 125,001 (Figure 8.10, Figure 8.11). The final change of inelastic stiffness was a 20% reduction from 25 kip/in. to 20 kip/in. While higher loads resulted in increased damage and loss of stiffness, CL2 performed well and did not fail during the test program.

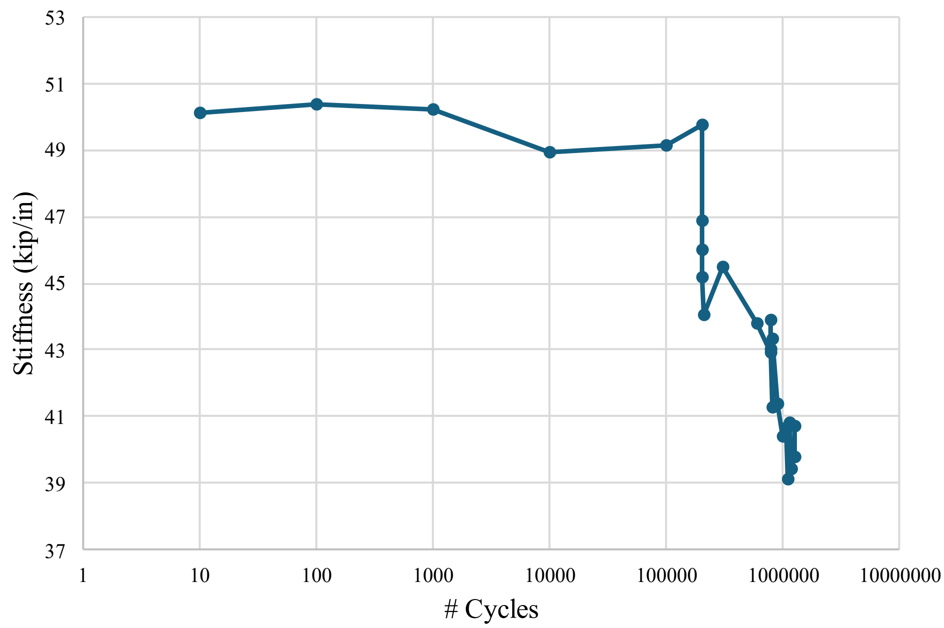

Figure 8.10 CL2: Elastic stiffness (3 to 9 kips) vs. completed cycles.

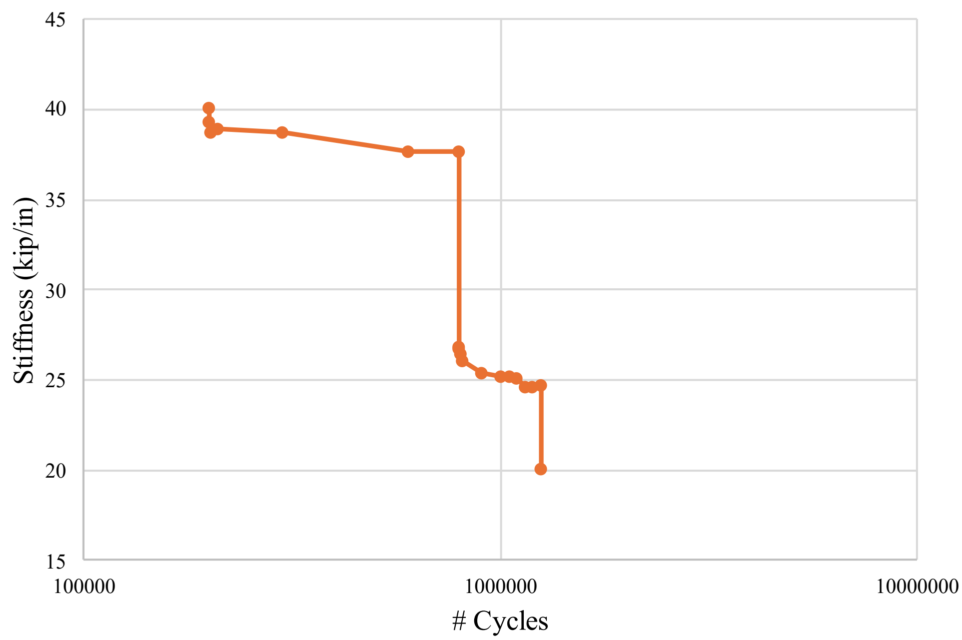

Figure 8.11 CL2: Inelastic stiffness (9 kips to maximum load) vs. completed cycles.

8.7 Practical Implications

Specimen CL1 failed after 619,028 load cycles, after indications of distress (popping noise, large flexural crack) were observed at 584,380 cycles. The flexural crack that opened at 584,380 cycles had a residual width (in the unloaded condition) of approximately 0.035 inches. The crack corresponded to the location of the embedded steel hold-down device, which likely affected stress concentrations in the strands. Loading continued for another 34,648 cycles until flexural failure occurred due to strand rupture. For context, 34,648 cycles corresponds to approximately 20 months of trucks for the average channel bridge and 1.5 months of trucks for the channel bridge with the maximum traffic (Table 8.1).

Repetitive loading had a significant impact on the flexural capacity of CL1. Failure corresponded to an experimental moment of 138 kip-ft. (including self-weight and applied load). In comparison, specimen L1 (Chapter 7), the weakest of the LMC-topped channels that were tested under static load, failed at an experimental moment of 228 kip-ft. Thus, CL1 had 40% less experimental capacity than the worst-performing specimen from static testing.

These results highlight the criticality of flexural cracks near the midspan of skinny-leg channel girders. Flexural cracks at this location may provide early signs of a channel's vulnerability to strand rupture and failure below nominal capacity. Specimen CL1 had an LMC topping; however, flexural cracks near midspan would also be a concern in untopped channel girders. The critical crack in CL1 had a residual width of approximately 0.035 inches.

Specimen CL2 did not experience the events that led to strand rupture in CL1. This result suggests that in the absence of other issues, the LMC topping can remain bonded with the channel through years of service-level truck loading.

8.8 Conclusions

Two skinny-leg channel girders with LMC topping, specimens CL1 and CL2, were tested under repetitive loads. The test setup was designed to produce bending moments equivalent to the effects of H15 or HL-93 trucks. Key conclusions and observations are listed below.

For specimen CL1:

- A popping sound indicating a strand or wire break was heard during cycle 384,380 of H15-equivalent loading. At the same time, a flexural crack with a residual width of ~ 0.035 in. was observed at midspan of one of the stems.
- Specimen CL1 failed due to strand rupture after 419,028 cycles of H15-equivalent load, or 34,638 cycles after the initial wire break. In terms of service time, 34,638 cycles correspond to 52, 38, and 20 months for average, 80th percentile, and 90th percentile of truck traffic, respectively.
- The experimental bending moment at failure was 138 kip-ft, which is 40% less than the worst-performing specimen from the quasi-static testing in Chapter 7.
- The LMC-topping partially delaminated due to the strand break and failure but otherwise stayed bonded throughout the test program.

For specimen CL2:

- Specimen CL2 supported 1,300,000 load cycles, including HL-93-equivalent loads without LMC delamination.

CHAPTER 9: FIELD TESTS OF RETROFITS FOR FLAT SLAB BRIDGES

While this report primarily focuses on channel girder bridges, this chapter presents the results of fieldwork conducted to evaluate retrofits for flat slab bridges. This is a follow-up to the lab work presented in a previous report for the SCDOT funded project, SPR 752 *Safe and Cost-Effective Reduction of Load Postings for South Carolina Bridges*. The background information in section 9.2 summarizes relevant information from SPR 752 (Ziehl et al., 2023).

9.1 Summary and Key Takeaways

- Retrofits involving near-surface-mounted (NSM) bars and FRP 'biscuits' were evaluated through field testing on an out-of-service flat slab bridge.
- By connecting adjacent slabs together, the biscuits improved distribution between the connected slabs by approximately 35% and attracted loads into the curb sections.
- By creating structural continuity between adjacent spans, the NSM bars reduced deflections in the connected slabs by 36% or more.
- The FRP biscuits required approximately less effort to install than the NSM bars.

9.2 Background

South Carolina has approximately 3,000 slab bridges with an average age of 58 years, as reported by the National Bridge Inventory (NBI 2024). The bridges were originally designed to carry H10 or H15 trucks, with typical cross sections shown in Figure 9.1.

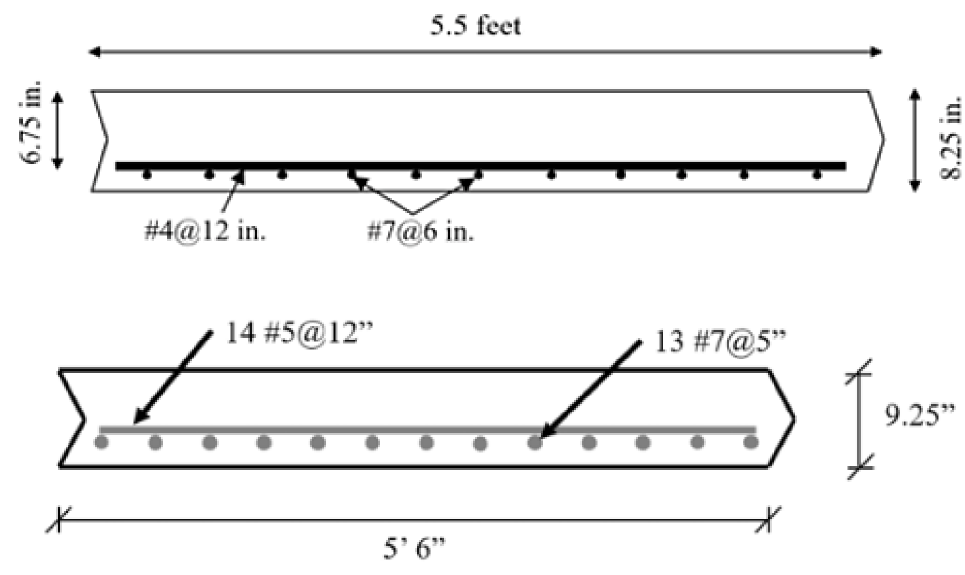

Figure 9.1 Flat-slab cross-sections for H10 (top) and H15 (bottom) truck loads.

As a part of SPR 752, laboratory tests were conducted to evaluate various retrofit strategies for improving the flexural capacity of flat slab bridges. The retrofits were categorized as either 'above-slab' or 'below-slab'. Above-slab retrofits included steel plates or channel sections bolted to the top of the slab as well as near-surface-mounted (NSM) bars installed to create continuity between adjacent spans (Figure 9.2). Below-slab retrofits consisted of bolted steel plates, external post-tensioning, and bonded FRP strips. These approaches are more efficient in terms of materials required. However, such systems are generally more difficult to install due to the need for access from below. The retrofits improved flexural capacity by 4% to 41% relative to baseline slabs.

Figure 9.2 Lab specimen with near-surface mounted (NSM) bars.

Field testing of a South Carolina flat-slab bridge was reported by Crabtree et al. (2021). The worst-case experimentally measured distribution factors for the moment ranged between 0.43 and 0.51 for interior slabs, depending on the slab and truck position.

9.3 Approach, Timeline, and Methodology

Based on the successful laboratory tests, NSM retrofit (Figure 9.2) was selected for field testing. A retrofit method involving carbon fiber-reinforced polymer (FRP) ‘biscuits’ was also selected. The biscuits are produced by V2 Composites (Figure 9.3). They are installed in grooves cut across the joint between adjacent slabs (Figure 9.4) with the intention of improving load distribution.

Figure 9.3 V2 composites T-biscuit.

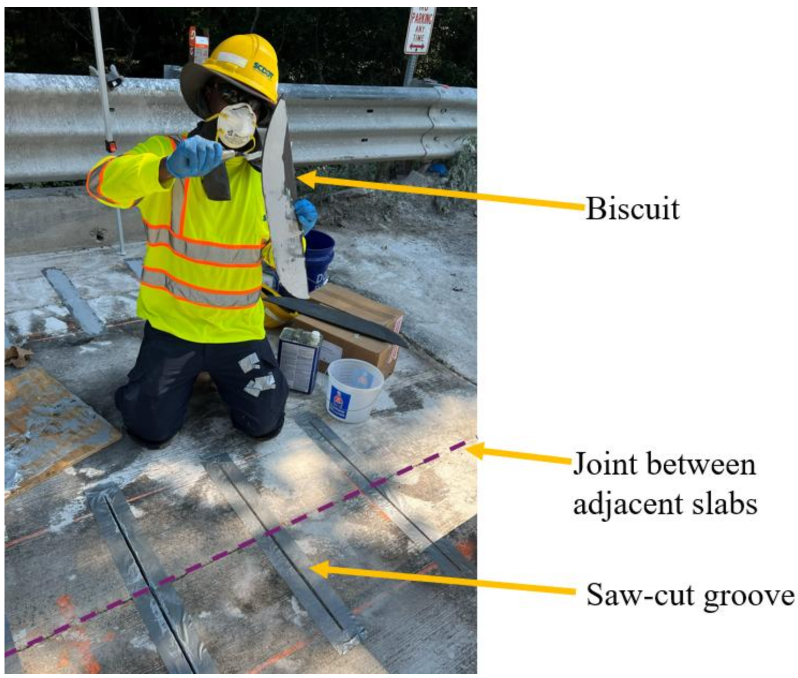

Figure 9.4 Installation of biscuits in saw-cut grooves.

The effectiveness of the retrofits was assessed through live-load field testing conducted both before and after retrofits were installed. A comparative analysis of the pre- and post-retrofit test results was performed to evaluate improvements (if any) resulting from the retrofits. Key dates of the project are summarized in Table 9.1.

Table 9.1 Key dates for installation and testing of flat-slab bridge.

Date	Task Completed
2/26/2025	As-is live load test
4/22/2025	Mock-up retrofit installation
6/23/2025	Bridge retrofit installation
7/23/2025	Post-retrofit live load test

The Four Hole Swamp Bridge in Dorchester, South Carolina, served as the testbed for evaluating the performance of the proposed retrofits. The bridge (Asset ID: 5036) consists of twenty-five 15-ft. spans (Figure 9.5). It was closed to traffic due to a timber pile failure. Field testing was conducted away from the failed pile using the three spans closest to the East Abutment. The bridge was originally built in 1967 and is scheduled for replacement.

Figure 9.5 Four-hole swamp bridge (left) and pile failure (right).

Live load was provided by an SCDOT truck loaded with gravel. The weight of each axle was measured on-site by the South Carolina State Transport Police using a portable scale. The weight and geometry are shown in Figure 9.6. The truck was driven across the bridge along five designated paths (Figure 9.7). These truck paths were chosen to represent possible truck locations while also ensuring that each individual slab was loaded and mirrored across the centerline of the bridge. Each of the truck paths was repeated three times to ensure data consistency.

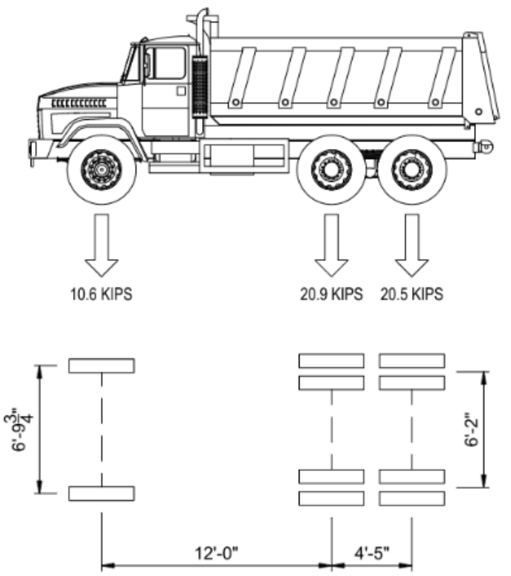

Figure 9.6 Truck weight and geometry.

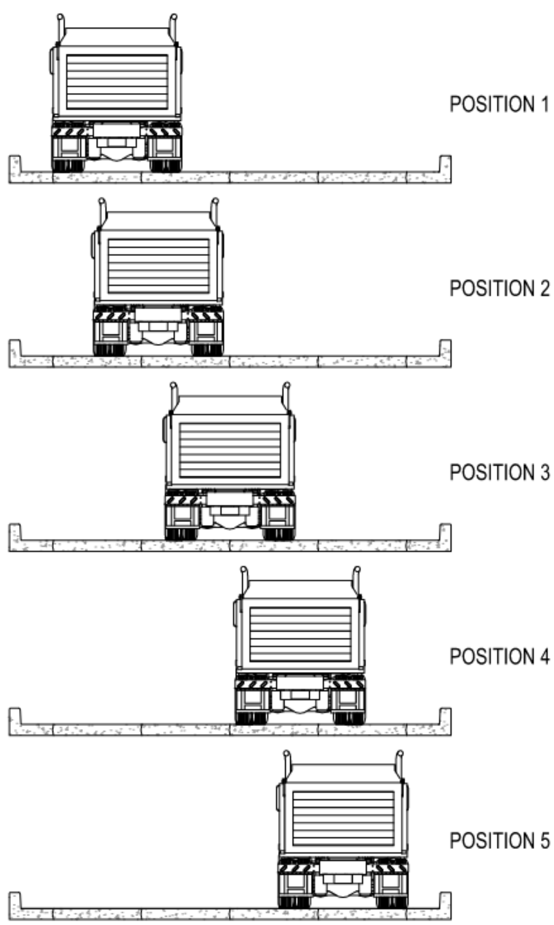

Figure 9.7 Truck crossing positions.

String potentiometers were used to measure the displacement of individual slabs as the truck crossed the test spans. The layout of the instrumentation and sensor locations is detailed in Figure 9.8. A wood frame was built between the timber piles on the second span to support the instruments located over water. Mounting blocks were adhered to the underside of the slabs and the instruments were mounted to the wood frame or to 4 in. x 4 in. lumber sitting on the ground. A wire line was used to connect the mounting blocks to the instruments and a plumb bob was used to ensure alignment.

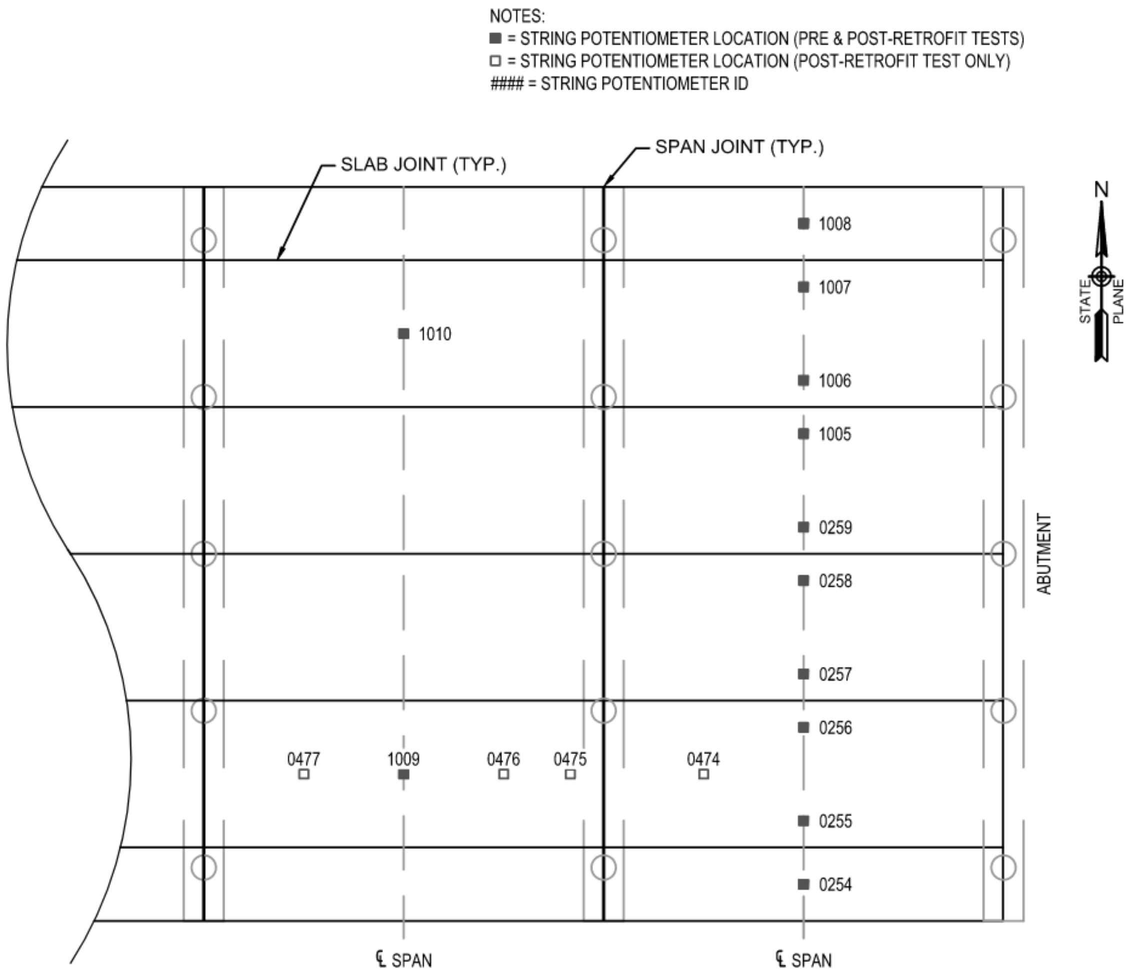

Figure 9.8 Instrumentation plan.

9.4 Results – Baseline Test

Figures 9.9 and 9.10 show the measured displacements from the baseline test for two of the truck positions. Data in the figures are based on the 'critical time', which corresponds to the maximum displacement measured during the given truck crossing. Data from all truck positions are presented later in the chapter where they are compared with the post-retrofit results. There was substantially less distribution in the baseline condition as evident from the uneven displacements shown in Figures 9.9 and 9.10. The slabs directly loaded by the truck displaced significantly, relative to the slabs located away from the truck, which showed little to no displacement. Additionally, the curb members at the edges of the span displaced little.

The displacement data were used to quantitatively determine the experimental distribution factors for the first span using Equation 9.1. This equation accounts for the differences in moment of inertia between the interior slabs and exterior curb members. In cases where slabs were instrumented with two string potentiometers the measurements were averaged for the calculations.

The calculated distribution factors for the baseline bridge conditions are presented in Table 9.2. The worst-case distribution factors are consistent with those reported by Crabtree et al. (2023) for a different flat-slab bridge.

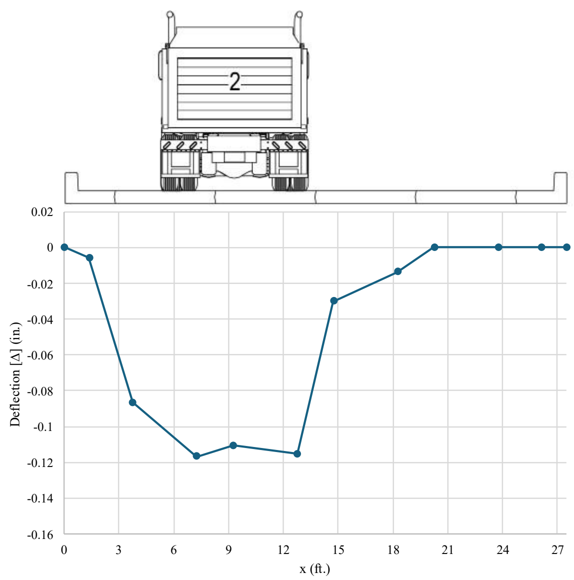

Figure 9.9 Span 1 displacement for truck position 2, baseline condition.

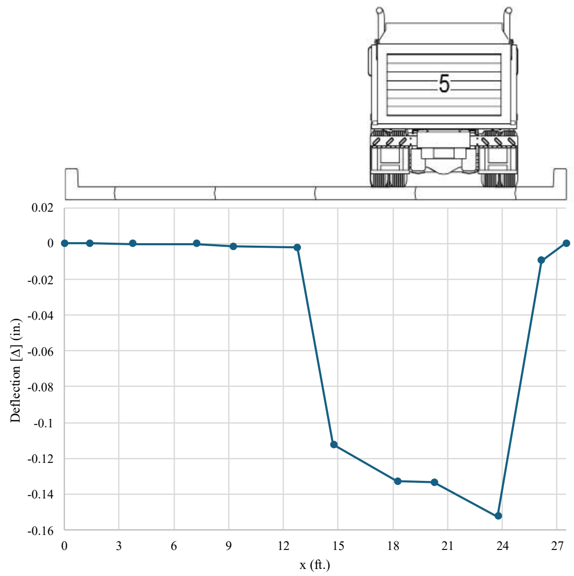

Figure 9.10 Span 1 displacement for truck position 5, baseline condition.

$$DF = \frac{I_i \Delta_i}{\Sigma(I_i \Delta_i)} \qquad \text{Equation 9.1}$$

Where:

DF = Distribution factor for moment

I_i = Moment of inertia of member i

Δ_I = Experimental displacement of member i

Table 9.2 Experimental distribution factors for baseline condition (bold and underline indicates the worst case for each member).

	Truck Position				
Member	1	2	3	4	5
Curb 2	**0.27**	0.03	0.00	0.00	0.00
Slab 4	0.35	**0.44**	0.03	0.00	0.00
Slab 3	0.36	**0.46**	**0.46**	0.03	0.01
Slab 2	0.04	0.08	**0.48**	0.46	0.44
Slab 1	0.00	0.00	0.02	0.47	**0.49**
Curb 1	-0.01	0.00	0.00	0.03	**0.06**

9.5 Retrofit Details and Installation

Following the baseline load test, portions of the bridge were retrofit with NSM bars or biscuits (Figures 9.11 and 9.12). The biscuits were installed on the first span and connected curb 2, slab 4, and slab 5. The NSM bars were installed to connect slab 1 in the first, second, and third spans.

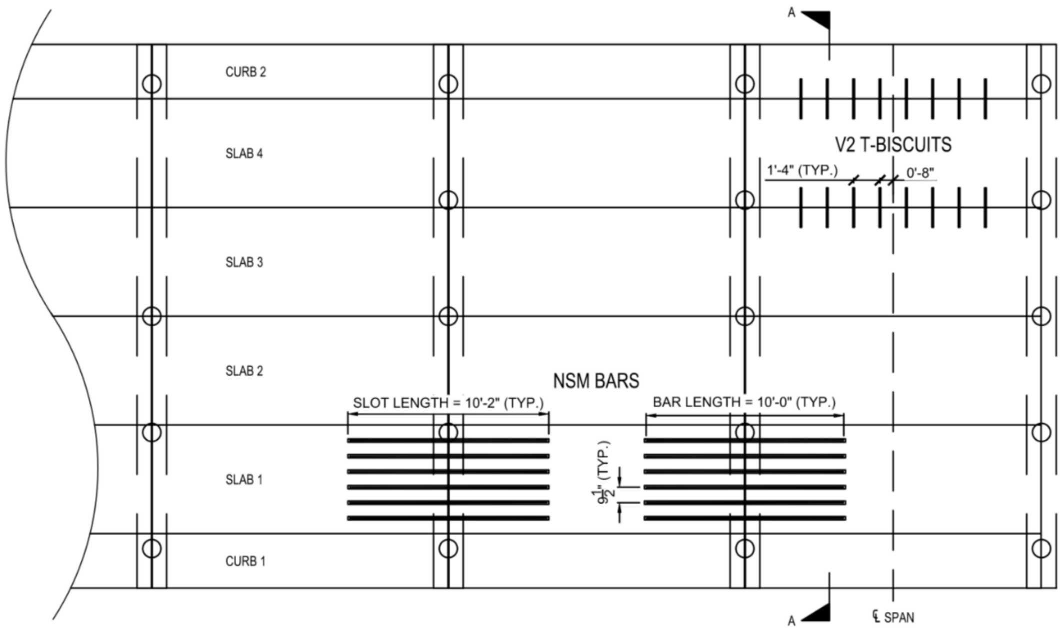

Figure 9.11 Plan view of flat-slab bridge retrofits.

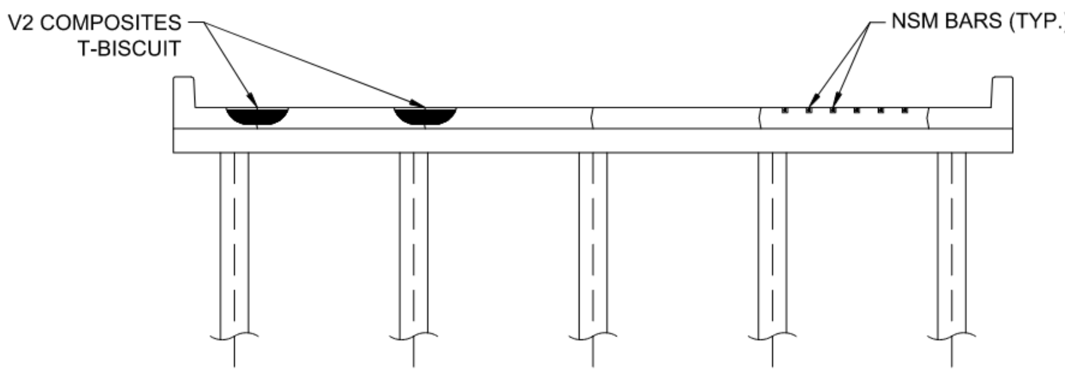

Figure 9.12 Cross-section of flat-slab bridge retrofits.

9.5.1 Material Properties

The biscuits were a proprietary fiber-reinforced polymer (FRP) material provided by V2 Composites. The data sheet of the manufacturer states that the biscuit is made of a tri-axial carbon fabric with proprietary textured glass fabric bonded to the exterior. The Z axis is through the thickness of the biscuit and the X and Y axes are in-plane. Their orientation relative to the fibers is not reported. According to the manufacturer, the T-biscuit material has a compressive strength of 52,585 psi along the X and Y axes, a tensile strength of 110,630 psi along the X and Y axes, and an in-plane shear strength of 20,992 psi along the Z axis. The FRP biscuits are bonded to the concrete using a proprietary adhesive paste and have a reported bond strength of 2,760 psi. The V2 Composites T-biscuits have been used in parking garage and lighthouse repair applications according to case studies reported by the manufacturer [*https://v2tbiscuits.com/#case-studies*]. The use of FRP biscuits for highway bridges has not been reported to our knowledge.

The data sheet reports an ultimate vertical shear capacity of eight kips and a design capacity of six kips for typical biscuits in 5,000 psi concrete. It is not clear what failure modes were considered and how they relate to the reported capacity. Typical biscuit dimensions are approximately 3.5 in. tall by 18 in. long, but the dimensions were modified for the slab bridge in this study. The biscuits used for this application were 5 in. tall by 24 in. long by 0.18 in. thick. The biscuits were installed in a 0.25 in. wide saw cut and adhered to the sides of the slot using the V2 biscuit bond paste provided.

The NSM bar retrofits were No. 5 rebars provided by SCDOT. The material specifications were not recorded; however, the NSM bars in the study only support service-level loads, so the steel grade was not a primary concern. Uncoated bars were used to minimize costs; however, for practical use, epoxy-coated or FRP bars may provide superior durability. The bars were placed in grooves that were 2 in. wide by 2 in. deep and backfilled with cementitious grout, which was also provided by the SCDOT. The cementitious grout used was QUIKRETE® non-shrink precision grout, which has a reported 28-day compressive strength of 8,000 psi for the specified fluid consistency [https://www.quikrete.com/productlines/nonshrinkprecisiongrout.asp].

9.5.2 Retrofit Design Approach

Distinct design approaches were used for the biscuits and the NSM bars. The biscuits are intended to improve load distribution between different slabs within a span, while the NSM bars were intended to create continuity of the slabs across spans. In both cases the goal was to improve bridge performance and potentially remove load postings.

The height of the biscuits and the depth of the slots were sized to fit the geometry of the slabs while avoiding the flexural reinforcement in the bottom of the slab. A 5.5 in. slot depth and a 5 in. biscuit height provided adequate clearance to avoid flexural reinforcement and for ½ in. of cover over the top of the biscuit.

The biscuit spacing was determined through discussions amongst the research team and was informed by the available strength data from the manufacturer. Specifically, a design capacity of six kips for a biscuit in 5,000 psi concrete. Although biscuits in the current application were larger than the manufacturer's standard the design value of six kips was used. A typical H15 truck has a rear axle weight of 24 kips. This load is spread between one set of tires on each end of the axle. Therefore, the target shear capacity is half of the total rear axle weight, equal to approximately 12 kips. At 12 kips of required shear capacity two biscuits would be sufficient. The research team decided to space the biscuits so that a minimum of two or three biscuits would be near the influence area of a tire patch within the high moment regions of the span. Using this approach, eight biscuits spaced at 16 in. on center and centered about midspan were used.

The near-surface mounted (NSM) bar retrofit was adapted from a previous lab test reported in SPR 752. Three significant differences were made between the lab test and the field implementation. First, the field study used No. 5 bars rather than the No. 6 bars used in the lab tests. Second, the field study included three back-to-back spans rather than two. Third, the joint between the adjacent spans was left as-is in the field study. In contrast, the joint was cleaned and filled for the laboratory test.

Cleaning and filling the joint between spans would have closed the approximately ½ in. gap between the slab ends, thereby allowing compression forces to transfer across the joint. Recognizing the effort required to clean and grout the slots, the research team decided against these steps in the field study; thus, the results are considered a lower bound of the potential for the NSM retrofit. If the NSM bars proved effective without joint preparation, they would be more economically viable in future applications. Installation of the NSM bars – even without cleaning and grouting the end joints – required more time and effort than biscuit installation.

9.5.3 Installation

Locations for the biscuits and NSM bars were marked with paint to ensure they would not be washed away by the water used for saw cutting. The biscuits required a ¼ in. groove, which was cut using double-stacked 1/8 in. blades on a Husqvarna FS 524 concrete saw. After cutting, the grooves were cleaned with a pressure washer and allowed to dry overnight. The following morning, duct tape was placed around each groove to facilitate cleanup after the biscuit and adhesive had been installed. A two-part epoxy paste provided by the biscuit manufacturer was mixed and inserted into the slots and used to coat the sides of the biscuits. The biscuits were inserted into the slots until their tops were at least ½ in. below the face of the concrete surface (Figure 9.12). The top was finished to be flush with the concrete surface and the tape was removed.

Figure 9.12 Cutting grooves (left) and installing biscuits (right).

A two-person crew prepared and installed the biscuits. The installation time per biscuit was approximately 40 minutes, including preparation and layout (10 minutes), cutting (15 minutes), pressure washing (5 minutes), placing tape and mixing the adhesive (5 minutes), and placing biscuits and finishing the top surface (5 minutes). Expanding these times to an entire span (8 biscuits per joint, 5 joints), it would take approximately 54 person-hours to retrofit an entire bridge span.

NSM bar installation involved cutting 10 ft. - 2 in. long by 2 in. wide by 2 in. deep slots in slabs across back-to-back spans. Each slot required three separate cuts: one along each edge and one down the center of each slot using a Husqvarna FS 524 concrete saw. The cuts were then pressure-washed and allowed to dry overnight. After the slots were sufficiently dry, a hammer drill with a two in. chisel attachment was used to break out the concrete between the cuts and remove any high spots that remained along the bottom of the slot. A leaf blower was then used to clean dust and debris from the slots immediately before the bars and grout were placed. A 10 ft. long No. 5 rebar was placed in each slot and the slot was filled with high-strength grout (Figure 9.13).

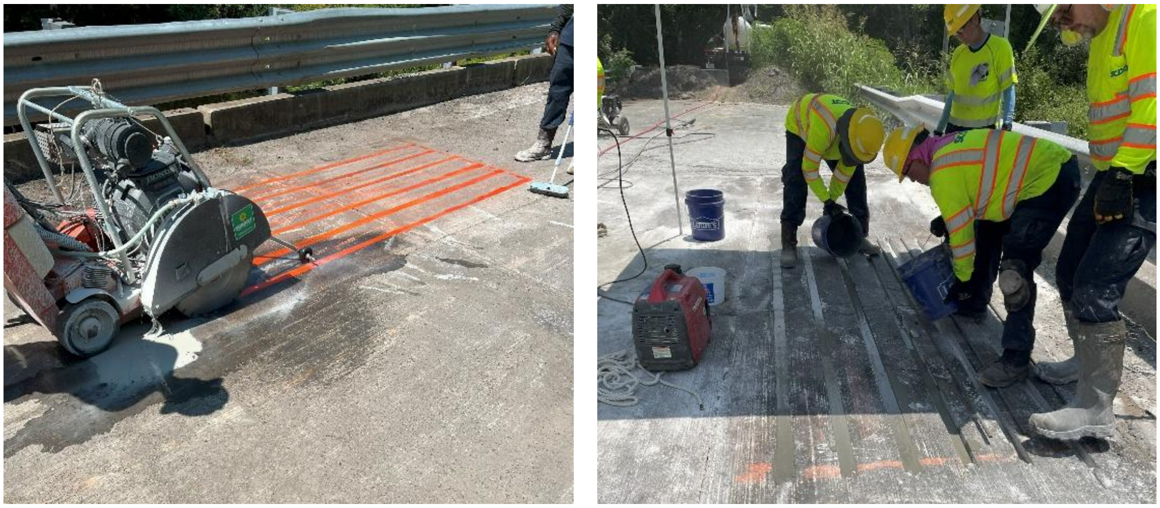

Figure 9.13 Cutting slots (left), NSM bar and grout installation (right).

A three-person crew installed the NSM bars. Tasks associated with an individual NSM bar took approximately 75 minutes, broken down to preparation and layout (15 minutes), cutting and chiseling slots (35 minutes), cleaning slots (five minutes), mixing grout (five minutes), placing grout and bars (10 minutes), and finishing the top surface (five minutes). A span-to-span joint includes four slab-slab connections, each with six bars. Based on these times and quantities, approximately 90 person-hours would be required to install NSM bars across an entire span-span joint.

The number of span-to-span joints in a bridge is equal to the number of spans minus one. If the relationship is simplified to one span to span joint per span, the biscuits required approximately 40% less effort to install (54 versus 90 hours) than the NSM bar retrofit.

9.6 Comparison of Baseline and Post-Retrofit Bridge Response

The post-retrofit data was processed using the same approach as the baseline data. The 'critical' times associated with maximum deflections were determined for each truck position. Measurements from the critical times were then used to calculate the experimental distribution factors using equation 9.1. A summary of the post-retrofit distribution factors is presented in Table 9.3.

The retrofits had a significant impact on the distribution factors for some members and truck positions but not for others (Table 9.4). Except for truck position 1, almost no load is distributed to curb 2. In contrast, curb 1 experienced a significant increase in distribution for truck position 5 following the retrofit. This is due to the biscuits, which tied curb 1 to slab 1, thereby sending more force to the curb. Changes in the load distributed to slabs 1 and 2 are also attributed to the biscuits.

Comparing distribution factors for slab 4 is not relevant because equation 9.1 does not account for changes to stiffness resulting from modified boundary conditions, such as the addition of NSM bars for continuity with the adjacent span.

Table 9.3 Experimental post-retrofit distribution factors (bold and underlined values indicate the worst cast value for each member).

	Truck Position				
Member	1	2	3	4	5
Curb 2	**0.26**	0.00	-0.01	-0.01	0.00
Slab 4	**0.33**	0.19	0.04	0.02	0.01
Slab 3	0.36	0.36	**0.45**	0.41	0.03
Slab 2	0.04	0.29	**0.31**	0.29	0.30
Slab 1	0.01	0.10	0.14	0.17	**0.27**
Curb 1	0.00	0.05	0.08	0.12	**0.40**

Table 9.4 Change in distribution factors from baseline to post-retrofit tests (bold and underlined values indicate the largest change for each member. Positive values indicate a higher distribution factor in the post-retrofit test).

	Truck Position				
Member	1	2	3	4	5
Curb 2	-0.01	**-0.03**	-0.01	-0.01	0.00
Slab 4	-0.02	**-0.25**	0.01	0.02	0.01
Slab 3	0.00	-0.10	-0.01	**0.38**	0.02
Slab 2	0.00	**0.21**	-0.17	-0.17	-0.14
Slab 1	0.01	0.10	0.12	**-0.30**	-0.22
Curb 1	0.01	0.05	0.08	0.09	**0.34**

Measured deflections from the baseline and post-retrofit tests are plotted together in Figures 9.14 to 9.18. Based on the orientation of the figures, the biscuits were installed on the right side of the bridge cross-section. Data from truck paths 4 and 5 (Figures 9.17 and 9.18) are most suitable for evaluating the impact of the biscuits. The decreased displacement of interior slabs in the post-retrofit test indicates that the biscuits improved load distribution. Comparing the worst-case distribution factors for the baseline and post-retrofit tests (Tables 9.2 and 9.3), the biscuits resulted in a 35% reduction (from 0.48 to 0.31) in the distribution factor for slab 2 and a 45% reduction (from 0.49 to 0.27) for slab 1.

The improved performance of the slabs with the biscuit retrofit is partially attributed to engagement with curb 1. The increase in displacement of curb 1 (Figure 9.18), indicates that the biscuits engaged the curb section. Even though the curb section was not directly loaded the biscuit connection allowed the curb to attract load away from the interior slabs. While curb 1 received little to no load from truck positions 4 and 5 in the baseline test, the measured deflections suggest that it attracted approximately 2.5 times more load after the biscuits were installed.

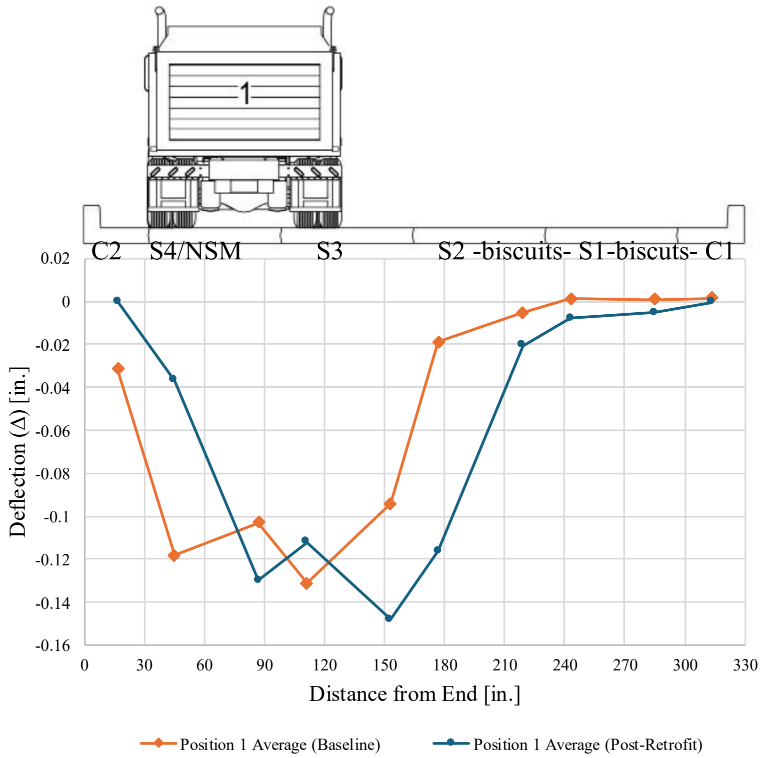

Figure 9.14 Span 1 baseline and post-retrofit displacements for truck position 1.

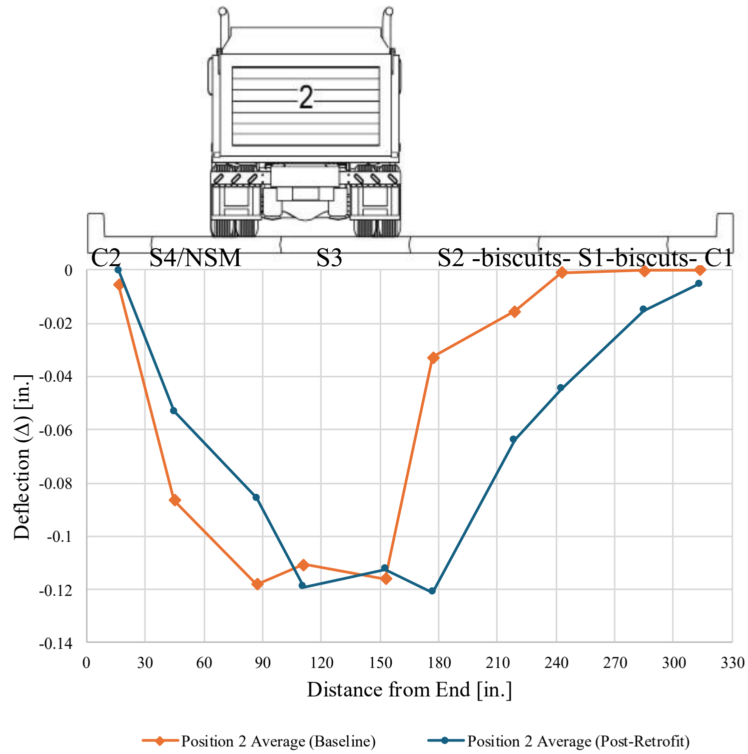

Figure 9.15 Span 1 baseline and post-retrofit displacements for truck position 2.

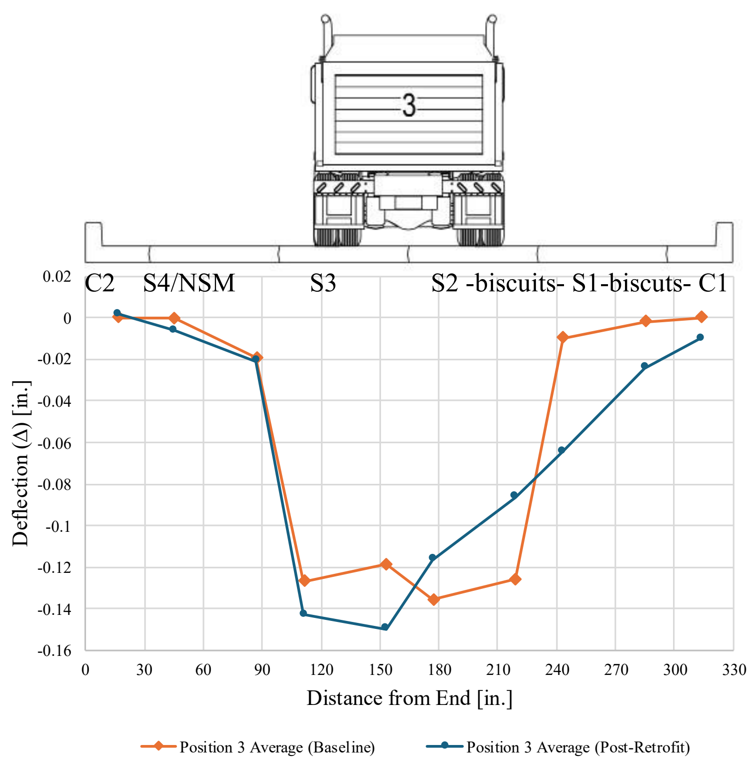

Figure 9.16 Span 1 baseline and post-retrofit displacements for truck position 3.

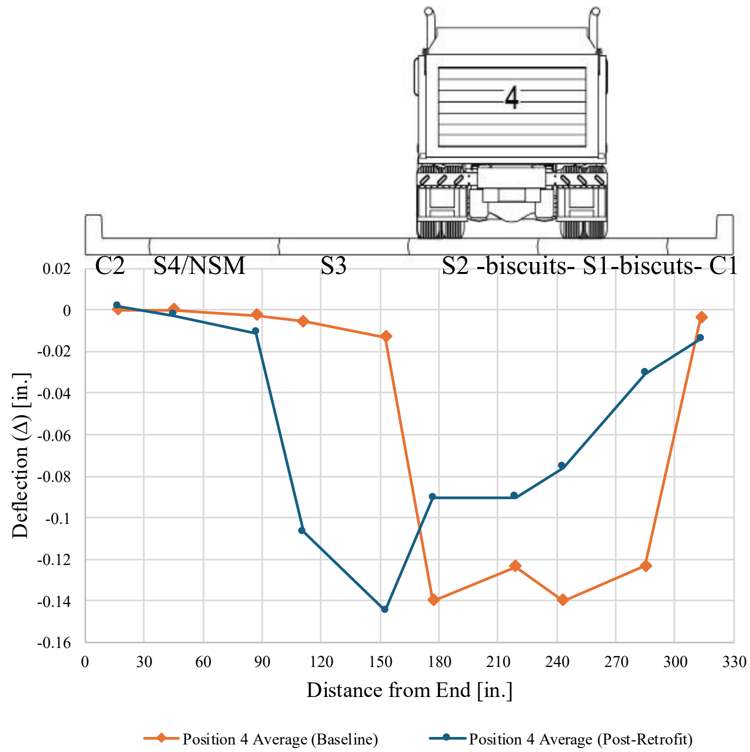

Figure 9.17 Span 1 baseline and post-retrofit displacements for truck position 4.

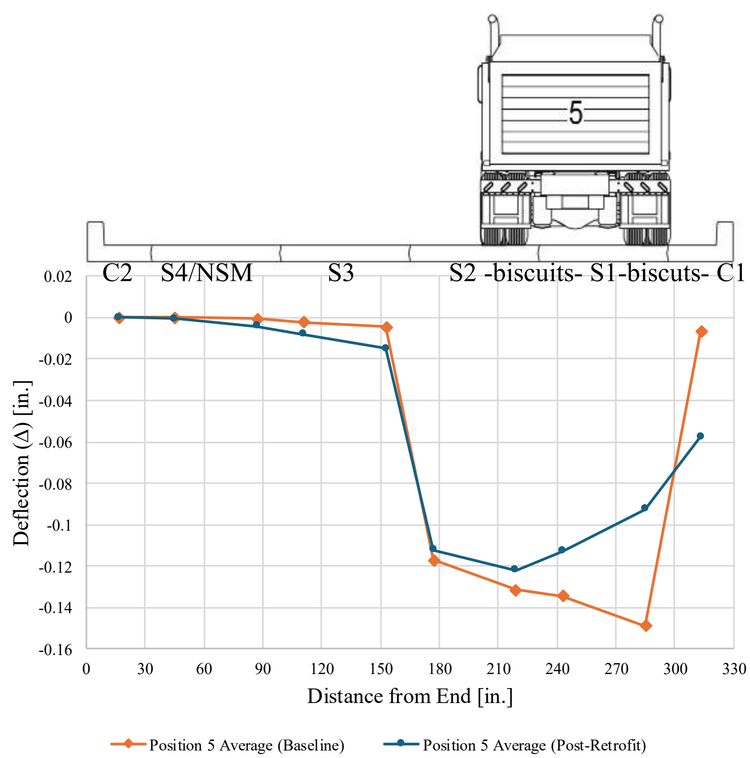

Figure 9.18 Span 1 baseline and post-retrofit displacements for truck position 5.

The slabs with NSM bars (slab 4) were directly loaded when the truck crossed at position 2. Measured displacements for these slabs and truck location are shown in Figure 9.19. The data in the figure correspond to the 'critical time' at which slab 4 in span 1 had the largest displacement. Figure 9.20 shows data from the same slabs and instruments, but at the critical time for slab 4 in span 2. Displacement data from the critical times of the baseline test are included in the figures.

For the orientation in Figures 9.19 and 9.20, the front of the truck was pointed to the right. At the critical time for span 1, the heavier back axle was on span 1, and the lighter front axle was on span 2. During the critical time span 2, no direct loads were applied to span 1. Thus, span 1 shows negligible displacement in Figure 9.20.

The NSM bars increased the stiffness of the #4 slabs, as indicated by the reduced displacement in the post-retrofit condition. The NSM bars resulted in a 36% reduction (from 0.11 to 0.07 inches) in maximum displacement in span 1 and a 68% reduction (from 0.038 to 0.012 inches) in span 2. The greater effect in span 2 is attributed to having NSM bars connecting adjacent spans at both ends, whereas at one end of span 1 there was an abutment and no adjacent span to connect to.

Even without cleaning and grouting the joints between spans, the NSM bars created a degree of continuity between the spans. It is likely that friction between the slabs and pier caps provided a load path for compressive forces to transmit across the joint while the NSM bars transmitted tensile forces.

The field results are consistent and complementary to lab tests of NSM bar retrofits from SPR-752. The lab testing demonstrated a 24% improvement in flexural capacity (Ziehl et al. 2023), and the field testing demonstrated a 36% to 68% increase in stiffness under service-level loads.

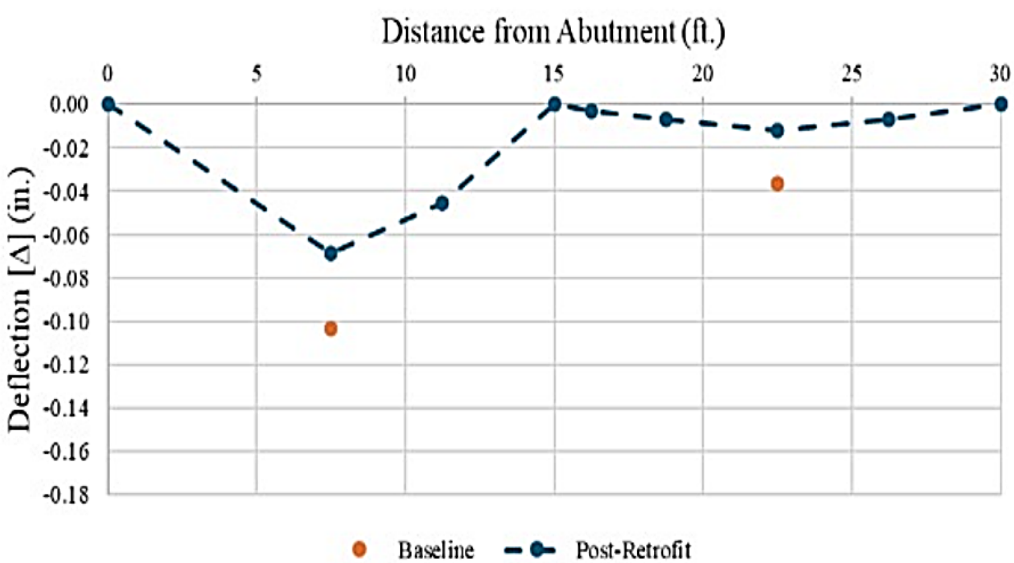

Figure 9.19 Deflections in slabs with NSM bars at the critical time in span 1.

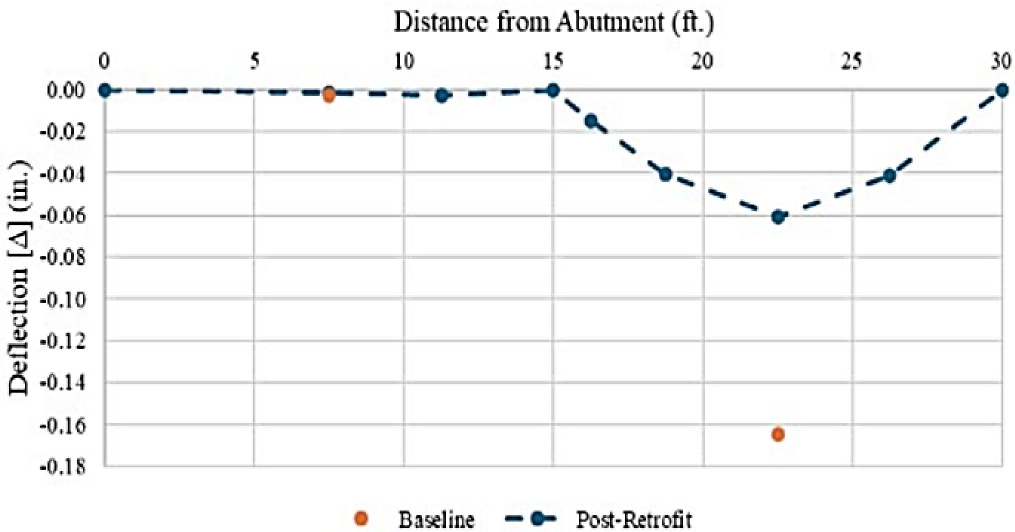

Figure 9.20 Deflections in slabs with NSM bars at the critical time in span 2.

9.7 Recommendations

While the field tests evaluated the performance of biscuits under service loading, additional work is recommended to determine the strength of the biscuit and slab members as a system. Lab tests should include monotonic loading to determine system capacity and controlling failure mode, as well as cyclic loading to evaluate performance through truck loads. With this information available, there may be an opportunity to reduce the installation effort by optimizing the spacing of biscuits. After the structural capacity of the system is characterized, another field test should be conducted to study load distribution when biscuits are installed at the optimized spacing.

The effect (if any) of cleaning and grouting the span to span joints should be studied in combination with NSM bars. Cleaning and grouting would likely contribute to a greater level of continuity between connected slabs. A field test that includes installation of NSM bars across all slabs in multiple spans could also be investigated, as well as alternative materials such as glass fiber-reinforced polymer (GFRP) reinforcing bars or epoxy-coated rebar.

9.8 Conclusions

The T-Biscuits provided by V2 Composites improved the service-level performance (in terms of lateral load distribution) of the retrofitted slabs. The biscuits enhanced load distribution by providing enhanced mechanical connection between adjacent slabs, allowing loads to be better shared with neighboring slabs. The biscuits enhanced engagement with the curb section even though the curb was not directly loaded. As a result of this improved load sharing, the retrofitted slabs had lower deflections compared to those observed in the baseline test, demonstrating increased overall stiffness and efficiency of the retrofit. The biscuits improved load distribution in the associated slabs by 35% to 45%. The biscuits were also relatively quick to install, requiring approximately 40% less effort per span than the NSM bars. It is noted that experience with both systems may reduce the installation time in future applications.

The NSM bars increased the stiffness of the associated slab members, as evidenced by the reduced deflections in the post-retrofit test compared to the baseline test. The NSM bars reduced the maximum displacement in span 1 by 36% relative to the baseline. The effect was even greater in span 2, wherein the maximum displacement was reduced by 68% due to the NSM bars. The greater effect in span 2 is due to the NSM bars attaching it to spans 1 and 2.

CHAPTER 10: COST-BENEFIT COMPARISONS OF BRIDGE RETROFITS

10.1 Summary and Key Takeaways

- Benefit costs estimates indicate that the bolting approach used for strengthening with aluminum shapes was more efficient that bonding alone.
- Transverse post-tensioning was the more efficient than latex modified concrete overlays.
- Retrofits with carbon FRP biscuits and near surface mounted bars both provided an efficient means to increase performance when working from above.

10.2 Basis for Calculations

Unit costs for materials, labor, and equipment were obtained from various sources, with the report for SPR 752 (Ziehl et al., 2023) as the main source. For items not addressed in SPR 752, unit costs were based on lab specimen supply costs, online material costs, and online equipment rental costs. In a few cases costs were estimated by comparison with similar products and services. Labor times were based on the effort measured during the preparation of lab and field specimens. Construction labor costs were assumed to be $25/hour.

A direct cost of $2,400 per day was used to account for bridge and lane closures during retrofit installation. The number of days of closure was estimated based on material curing times, measured installation times during field and lab studies, and likely crew sizes. The daily cost of closure assumes 12 hours of active traffic control per day at $200 per hour. This rate is consistent with SPR 752 and includes "equipment and crews to … direct traffic." For the other 12 hours the calculations assume passive traffic control, utilizing signs and barriers. It is assumed that passive control incurs negligible direct costs.

Equations for calculating retrofit benefits are presented in Table 10.1. Data used in the benefit calculations depended on the aim of the retrofit (flexural strengthening or improved load distribution). However, the general approach was the same for both aims; benefit was taken as the ratio of performance with the retrofit to performance without it.

Table 10.1 Methods for calculating the benefit of retrofits.

Retrofit aim	$\boldsymbol{Benefit = performance\ ratio}$
Flexural strengthening	$\dfrac{Expiermental\ capacity\ of\ retrofit\ specimen}{Average\ experimental\ capacity\ of\ baseline\ (no\ retrofit)\ specimens}$
Improve load distribution	$\dfrac{Expiermental\ distribution\ factor\ before\ retrofit}{Experimental\ distribution\ factor\ after\ retrofit}$

10.3 Channel Girders

Costs and benefits were calculated for six different retrofit schemes for channel girders (Table 10.2). Costs were calculated for a four-span bridge. Each span was 30 ft. with 10 channel girders per span. After estimating total retrofit costs for the bridge, the costs were normalized to a per-span retrofit cost. Estimated construction times are listed in Tables 10.3 and estimated costs are listed in Table 10.4.

Table 10.2 Channel girder retrofit schemes in cost-benefit analysis.

Label	Description	Aim	Reference
SE	External aluminum attached with epoxy	Improve flexural strength	Chapter 4
SB	External aluminum attached with bolts	Improve flexural strength	
SEB	External aluminum attached with epoxy and bolts	Improve flexural strength	
LMC	Latex-modified concrete overlay	Improve load distribution	Chapters 5 - 8
XPT	Transverse post-tensioning	Improve load distribution	
LMC+XPT	Latex-modified concrete overlay and transverse post-tensioning	Improve load distribution	

Table 10.3 Estimated construction time for a four-span channel bridge.

Task	Construction Days					
	SE	SEB	SB	LMC	XPT	LMC + XPT
Installation of AA shapes	3	4	2	--	--	--
Pavement removal	--	--	--	1	--	1
LMC placement	--	--	--	2	--	2
LMC curing	--	--	--	4	--	4
XPT installation	--	--	--	--	1	1
Total	3	4	2	7	1	8
Total closure cost ($)	7,200	9,600	4,800	16,800	2,400	19,200

Table 10.4 Estimated cost per span for channel retrofits.

Category	Cost ($)					
	SE	SEB	SB	LMC	XPT	LMC + XPT
Materials	27,600	30,800	19,000	8,400	5,000	13,400
Labor	1,600	2,400	1,800	1,800	1,200	3,000
Equipment & tools	10,500	16,500	8,300	1,100	6,400	7,500
Pavement removal	0	0	0	4,080	0	4,080
Closure	7,200	9,600	4,800	16,800	2,400	19,200
Total direct costs	46,900	59,300	33,900	32,180	15,000	47,180
Cost per span ($)	11,725	14,825	8,475	8,045	3,750	11,795

Transverse post-tensioning (XPT) is the least costly retrofit scheme in the group. Installation of the XPT takes relatively little time and requires limited materials. The costliest option is attaching aluminum shapes to the channel webs using epoxy and bolts (SEB), which requires a substantial quantity of materials and has a relatively high equipment cost, including a snooper truck for installation work below the bridge.

Table 10.5 summarizes the benefits provided by the retrofit schemes. The benefits were calculated using the approach outlined in Table 10.1. For the channels strengthened by externally attached aluminum alloy, experimental flexural capacities were used to determine the benefits. The retrofitted channel specimens had different pre-test conditions, with SE having moderate damage and the others being in relatively good condition. To account for variable pre-test conditions the denominator of the performance ratio was taken as the average flexural capacity of non-retrofit specimens having the same condition as the test specimen. Damage and average capacities are discussed in Chapter 4.

Table 10.5 Benefits of channel retrofits.

Category	Benefit					
	SE	**SEB**	**SB**	**LMC**	**XPT**	**LMC+ XPT**
**Aim of retrofit	FC	FC	FC	LD	LD	LD
Flexural strength with retrofit (k-ft)	175	246	285	--	--	--
Flexural strength without retrofit (k-ft)	190	215	215	--	--	--
Interior distribution factor w/ retrofit	--	--	--	*0.176	*0.181	*0.176
Interior distribution factor w/out retrofit	--	--	--	*0.240	*0.240	*0.240
Exterior distribution factor w/ retrofit	--	--	--	0.222	0.241	0.227
Exterior distribution factor w/out retrofit	--	--	--	0.250	0.250	0.250
Performance ratio	1.09	1.14	1.33	*1.36	*1.33	*1.36
				1.13	1.04	1.10
% improvement	9%	14%	33%	*36%	*33%	*36%
				13%	4%	10%
Cost/performance ratio (lower is better)	10757	13004	6372	*5915	*2820	*8673
				7119	3606	10723

* Denotes values for interior channels
** FC denotes improved flexural capacity; LD denotes improved load distribution

The benefits of adding LMC topping and/or transverse post-tensioning were calculated using field measurements from both interior and exterior channels (Table 10.5). In comparison to the interior channels the retrofits had a lesser impact on the exterior channels; however, it is reasoned that the performance of the interior channels provides a better representation of the benefits. Interior channels are located directly below the drive lines and are more likely to support truck loads, whereas exterior channels are partially covered by curbs and guardrails and only indirectly support trucks. Depending on the bridge, eight or nine interior channels are present, and only two exterior channels.

Cost-benefit comparisons for the channel retrofits are presented in Figure 10.1 and at the bottom of Table 10.5. Due to its relatively low cost and high retrofit performance, transverse post-tensioning (XPT) is the most cost-effective of the schemes evaluated. It provides the most 'bang for the buck,' even when considering the lesser improvement provided to external channel girders. Of the schemes involving aluminum alloy strengthening, SB provides the highest value.

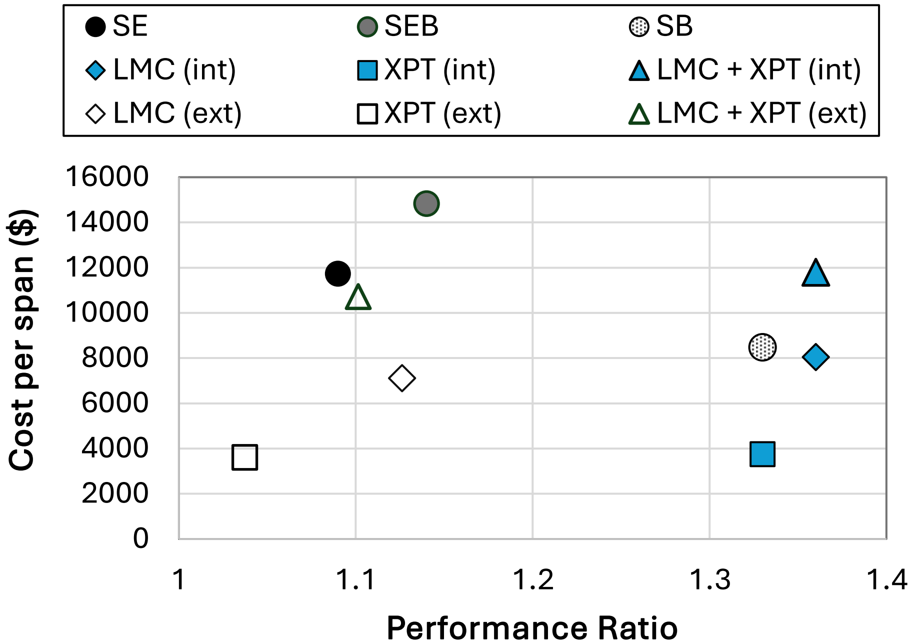

Figure 10.1 Cost-benefit comparison of channel retrofits. SE, SEB, and SB benefits are based on improved flexural capacity, whereas the others are based on improved load distribution.

10.3 Flat Slabs

Costs for the flat-slab retrofits were estimated for a bridge having eight 15 ft. spans. Each span had four interior slabs and two exterior curb members. Costs were calculated for the two retrofit methods considered in Chapter 9, NSM bars and biscuits. After the total costs were determined, they were divided by eight to determine the per span cost of retrofitting. Costs are summarized in Table 10.6.

Table 10.6 Costs for retrofitting an eight-lane flat slab bridge.

Category	**Cost x $1,000**	
	NSM Bars	**Biscuits**
Materials	11.5	30.0*
Labor	11.0	7.2
Equipment & tools	12.0	8.0
Pavement removal	4.0	4.0
Closure**	36.0	24.0
Total	74.5	73.2
Total per span	9.3	9.2
* Data not available, conservative assumption ** Based on 15 days for NSM bars and 10 days for biscuits		

Bridge closure costs account for approximately half of the total for the NSM bar retrofit and a third for the biscuits. The high closure costs are due to the fact that these schemes require work on top of the superstructure. Improved work efficiency, particularly time cutting slots and grooves, could have a significant impact on costs.

Cost data for the biscuits was not available. Therefore, a conservative assumption was made. Depending on the accuracy of the assumed biscuit cost, the total cost of the biscuit retrofit scheme could vary significantly from the estimate. Given the similarity of the tasks involved in installing NSM bars and biscuits it appears reasonable that the costs would be similar for both schemes.

The performance ratio (benefit) for the NSM bars was determined from the structural testing reported in SPR 752. The scheme aims to strengthen the slabs, and the performance ratio was calculated as the flexural capacity of the retrofit slab divided by the flexural capacity of a non-retrofit baseline slab. Although NSM bars were studied in the current project (Chapter 9), the data needed to calculate the performance ratio were only available from SPR 752.

The aim of the T-biscuits is to improve load distribution, and the performance ratio was calculated as the ratio of the experimental distribution factors. Because only a few members in the test bridge were retrofitted with T-biscuits, the performance ratio was determined from displacement data from slab 2 and truck position 5. The data from this slab and truck position yielded a performance ratio of 1.47. Slab 1 had higher performance ratios, but the lower value was chosen to be conservative in the cost-benefit evaluation.

A summary of cost-benefit comparisons for NSM bars and T-biscuits is provided in Table 10.7. The data used in the cost-benefit analysis for the flat-slab retrofits are based on sparse data and multiple assumptions. From the estimates presented in Tables 10.4 and 10.5, it can be concluded that installation time (work on the bridge deck), the cost of the biscuits, and the performance ratio of the biscuits have the greatest uncertainty and largest impact on the results.

Table 10.7 Cost-benefit comparisons of flat-slab retrofits.

	NSM Bars	**Biscuits**
Aim	Flexural strengthening	Improve load distribution
Baseline performance	208 kip-ft	0.44
Retrofit performance	257 kip-ft	0.30
Performance ratio	1.24	1.47
Cost/span ($ x 1,000)	9.3	9.2
Cost/performance ratio (lower is better)	7,510	6,354

10.4 Summary and Conclusions

The costs and benefits of the retrofit schemes described in earlier chapters were analyzed. While analyses provide information on the key drivers of costs they are based on sparse data and assumptions. Until additional data become available, caution is warranted when applying the results.

Conclusions for channel girder retrofits:

- Transverse post-tensioning (XPT) provided the greatest value of the retrofit schemes considered. XPT had the lowest estimated cost, as it requires limited materials and effort to install.
- Of the schemes with externally attached aluminum for strengthening, bolting (SB) provided the best value. Relative to bolting, attachment with epoxy increased the costs of materials, labor, and equipment, but did not provide additional performance benefits.

Conclusions for flat-slab retrofits:

- Both retrofit schemes, near-surface-mounted (NSM) bars and biscuits, involve similar work and have similar costs and cost-benefit ratios.
- The value of both schemes is impacted by construction time and associated costs for traffic control and bridge closure. For the NSM bar retrofit, closure costs accounted for 50% of the estimated total. Thus, optimizing the technical design to minimize construction time and improving construction efficiency will improve the value proposition of both schemes.

CHAPTER 11: CONCLUSIONS AND RECOMMENDATIONS

Evaluations of retrofit concepts considered in the project produced promising results. At the same time, additional design optimization, lab research, and/or further field trials are warranted.

Cost-benefit for channel girder retrofits:

- Transverse post-tensioning (XPT) provided the greatest overall value of the retrofit schemes considered. XPT had the lowest estimated cost, as it only requires limited materials and effort to install.
- Of the schemes with externally attached aluminum for strengthening, bolting (SB) provided the best value. Relative to bolting, attachment with epoxy increased the costs of materials, labor, and equipment, but did not provide additional performance benefits with the approaches considered.

Cost-benefit for flat-slab retrofits:

- Both retrofit schemes, near-surface-mounted (NSM) bars and biscuits, involve similar work and have similar costs and cost-benefit ratios.
- The value of both schemes is significantly impacted by construction time and associated costs for traffic control and bridge closure. For the NSM bar retrofit, closure costs accounted for 50% of the estimated total. Thus, optimizing the technical design to minimize construction time and improving construction efficiency would improve the value proposition of both schemes. Lane closures would likewise affect some of the approaches for strengthening from below the bridge in the event that a snooper truck is used.

.

References:

AASHTO (2017). AASHTO LRFD Bridge Design Specificatons, 8th edition, American Association of State Highway and Transportation Officials, Washington, DC, USA.

Aidoo J., Harries KA, and Petrou MF, *Full-scale experimental investigation of repair of reinforced concrete interstate bridge using CFRP materials.* Journal of Bridge Engineering, 2006. **11**(3): p. 350-358.

Al-Osta MA, Isa MN, Baluch MH, Rahman MK, *Flexural behavior of reinforced concrete beams strengthened with ultra-high performance fiber reinforced concrete.* Construction and Building Materials, 2017. **134**: p. 279-296.

Aykac S, Kalkan I, Aykac B, Karahan S, Kayar S, *Strengthening and repair of reinforced concrete beams using external steel plates.* Journal of Structural Engineering, 2013. **139** (6): p. 929-939.

Barker, RM, & Puckett, JA (2021). Design of Highway Bridges: An LRFD Approach. John Wiley & Sons.

Crabtree B, Ross BE, Cousins TE, Ziehl P, *Live-load Testing of Flat Precast Slab Bridge to Determine Joint Efficiency and Distribution Factors for Moment.* Journal of Performance of Constructed Facilities, 2021. **35** (1): p. 04020134.

Dodd S, (2023), *Effect of Latex Modified Concrete Overlays with Reduced Surface Preparation on the Load Distribution and Flexural Strength of Channel Girders*, MS Thesis, Clemson University.

Eubanks W, (2023), *Effect of Transverse Post-Tensioning on Moment Distribution Between Channel Girders*, MS Thesis, Clemson University.

Rasheed, HA, Abdalla, J, Hawileh, R, and Al-Tamimi, AK, *Flexural Behavior of Reinforced Concrete Beams Strengthened with Externally Bonded Aluminum Alloy Plates.* Engineering Structures, 2017. **147**: p. 473-485.

Sprinkel, Michael M. "Twenty-year Performance of Latex-modified Concrete Overlays." *Transportation Research Record,* 1992. 1335: p. 27-35.

Yang D, and Bradberry TE, *Texas' Use of CFRP to Repair Concrete Bridges.* ACI Symposium Publication. **277**.

Waters P, *Field Evaluation of Transverse Post-Tensioning and Latex Modified Concrete on Bridge Load Distribution*, Waters, Paige. Clemson University ProQuest Dissertations & Theses, 2024. 31895516.

https://v2tbiscuits.com/wp-content/uploads/2023/03/V2-T-Biscuit-Data-Sheet.pdf

https://v2tbiscuits.com/#case-studies.

https://www.quikrete.com/productlines/nonshrinkprecisiongrout.asp.